Antiferromagnetic order breaks inversion symmetry in a metallic double perovskite, Pb_2NiOsO_6

Antiferromagnetic order breaks inversion symmetry in metallic double perovskite, Pb_2NiOsO_6

Hai L. Feng,[1,2#] Chang-Jong Kang,[3,4#] Pascal Manuel,[5] Fabio Orlandi,[5] Yu Su,[6,7] Jie Chen,[6,7] Yoshihiro Tsujimoto,[6,7] Joke Hadermann,[8] Gabriel Kotliar,[3] Kazunari Yamaura,[6,7] Emma E. McCabe,[9, 10*] Martha Greenblatt[1*]

[1]Department of Chemistry and Chemical Biology, Rutgers, the State University of New Jersey, 123 Bevier Road, Piscataway, NJ 08854, USA

[2]Beijing National Laboratory for Condensed Matter Physics and Institute of Physics, Chinese Academy of Sciences, Beijing 100190, China

[3]Department of Physics and Astronomy, Rutgers, the State University of New Jersey, 136 Frelinghuysen Road, Piscataway, NJ 08854, USA

[4]Department of Physics, Chungnam National University, Daejeon 34134, South Korea

[5]ISIS facility, STFC, Rutherford Appleton Laboratory, Chilton, Didcot, Oxfordshire OX11 0QX, UK.

[6]International Center for Materials Nanoarchitectonics (WPI-MANA), National Institute for Materials Science, Tsukuba, Ibaraki 305-0044, Japan

[7]Graduate School of Chemical Sciences and Engineering, Hokkaido University, Sapporo, Hokkaido 060-0810, Japan

[8]EMAT, University of Antwerp, Groenenborgerlaan 171, 2020 Antwerp, Belgium

[9]School of Physical Sciences, University of Kent, Canterbury, Kent CT2 7NH, UK

[10]Department of Physics, Durham University, Lower Mountjoy, South Road, Durham, DH1 3LE, UK

[#] Hai L. Feng and Chang-Jong Kang contributed equally.

*Martha Greenblatt
greenbla@chem.rutgers.edu

*Emma E. McCabe
emma.mccabe@durham.ac.uk

Abstract: A Polycrystalline sample of Pb_2NiOsO_6 was synthesized by high-pressure (6 GPa) and high-temperature (1575 K) conditions. Pb_2NiOsO_6 crystallizes in a monoclinic double perovskite structure with a centrosymmetric space group $P2_1/n$ at room temperature. Pb_2NiOsO_6 is metallic down to 2 K and shows a single antiferromagnetic (AFM) transition at T_N = 58 K. Pb_2NiOsO_6 is a new example of a metallic and antiferromagnetic oxide with three-dimensional connectivity. Neutron powder diffraction and first-principle calculation studies indicate that both Ni and Os moments are ordered below T_N and the antiferromagnetic magnetic order breaks inversion symmetry. This loss of inversion symmetry driven by antiferromagnetic order is unusual in metallic systems and the 3d-5d double-perovskite oxides represent a new class of noncentrosymmetric AFM metallic oxides.

Introduction

The transition metal oxides (TMOs) exhibit unique correlations between magnetism and electrical conductivity: ferromagnetism (FM) in TMOs usually coexists with metallic conductivity, whereas insulating TMOs usually exhibit antiferromagnetism (AFM)[1]. Exceptions from this behavior, such as FM insulating oxides and AFM metallic oxides, are less common. $CaCrO_3$ and $Nb_{12}O_{29}$ are examples of AFM metallic oxide with three-dimensional crystal structures[2-4]. Other AFM metallic oxides such as $La_{2-2x}Sr_{1+2x}Mn_2O_7$ and $Ca_3Ru_2O_7$ crystallize in layered crystal structures and FM couplings are dominant within the layer[5, 6]. Recently, RuO_2, and $LaNiO_3$, which had been described as paramagnetic metals, were found to be AFM ordered and are new examples of AFM metallic oxides with three-dimensional crystal and electronic structures[7-9].

5d TMOs are unique correlated systems because of the spatial extent of the 5d electrons, generally giving 5d TMOs wider bandwidths (*W*), stronger spin-orbit coupling (SOC), and smaller on-site Coulomb repulsion (*U*) compared with 3d TMOs[10]. For instance, metal-insulator transitions driven by AFM orders were proposed in 5d oxides, Pb_2CaOsO_6[11], $Cd_2Os_2O_7$[12, 13], and $NaOsO_3$[14], and a ferroelectric-like structural transition breaking inversion symmetry has been observed in metallic $LiOsO_3$[15]. Recent studies on a 5d metallic oxide Pb_2CoOsO_6 demonstrated that the AFM order breaks inversion symmetry[16,17]. In this work we have built on this, synthesizing a new 5d hybrid double perovskite oxide Pb_2NiOsO_6 which is a new example of AFM metallic oxide. Characterization using neutron powder diffraction (NPD) and property measurements suggest that magnetic order breaks inversion symmetry (similar to reports on Pb_2CoOsO_6[16]). First-principle calculations confirm that both Ni and Os moments are ordered, allowing us to confirm the nature of the ground state (which has not been fully explored previously). The 3d-5d double-perovskite oxides establish a new class of noncentrosymmetric AFM metallic oxides, and our symmetry analysis of Pb_2NiOsO_6 explores how this understanding can be applied more widely to design new magnetoelectrics.

2. EXPERIMENTAL

Polycrystalline Pb_2NiOsO_6 was synthesized via a solid-state reaction from powders of PbO_2 (99%, Alfa), Os (99.95%, Heraeus Materials), NiO (99.997%, Alfa), and $KClO_4$ (99.99%, Alfa). The powders were thoroughly mixed in a stoichiometric ratio in an Ar-filled glove box, followed by sealing in a Pt capsule. The Pt capsule was statically and isotropically compressed in a belt-type high-pressure apparatus (Kobe Steel, Ltd., Japan [18]), and a pressure of 6 GPa was applied while the capsule was heated at 1400 °C for 1 h, followed by quenching to room temperature in less than a minute. The pressure was then gradually released over several hours.

A dense and black polycrystalline pellet was obtained, and several pieces were cut out from it. A selected piece was finely ground for a synchrotron X-ray diffraction (SXRD) study, which was conducted in a large Debye–Scherrer camera in the BL15XU beamline, SPring–8, Japan[19, 20]. The SXRD pattern was collected at room temperature and the wavelength was confirmed to be 0.65298 Å by measurement of a standard material, CeO_2. The absorption coefficient was measured in the same line. The SXRD data were analyzed by the Rietveld method with the RIETAN–VENUS software[21]. The crystal structure was depicted by VESTA[22].

The electrical resistivity (ρ) of a polycrystalline pellet of Pb_2NiOsO_6 was measured by a four-point method at a gauge current of 0.1 mA in a physical properties measurement system (PPMS, Quantum Design, Inc.). Electrical contacts were made with Pt wires and Ag paste in the longitudinal direction. The temperature dependence of the specific heat capacity (C_p) was measured in the same PPMS by a thermal relaxation method at temperatures between 2 and 300 K with Apiezon N grease thermally connecting the material to the holder stage.

The magnetic susceptibility (χ) of Pb_2NiOsO_6 powder was measured in a magnetic properties measurement system (MPMS, Quantum Design, Inc.). The measurement was conducted in field cooled (FC) and zero-field cooled (ZFC) conditions in the temperature range between 2 and 390 K. The applied magnetic field was 10 kOe.

Time-of-flight neutron powder diffraction data were collected at the WISH diffractometer (target station 2) at the ISIS Neutron and Muon Source.[23] For the neutron powder diffraction (NPD) data collection, 3.26 g of Pb_2NiOsO_6 powder were placed in a 6 mm diameter cylindrical vanadium can under helium and sealed using indium wire. The sample was loaded into a helium cryostat and cooled to base temperature (1.5 K). A high-quality data set was collected at 1.5 K (~ 1 hour, ~40 μAmp hr) and shorter scans (~ 15 minutes, ~10 μAmp hour) were collected every 2.5 K on warming to 100 K. A final higher quality scan (~ 1 hour, ~40 μAmp hour) was collected at 98 K in the paramagnetic phase. Data were analyzed and Rietveld refinements carried out using TopasAcademic,[24, 25] and the web-based ISODISTORT software[26] was used for symmetry analysis. Rietveld refinements for the antiferromagnetic system were carried out with a nuclear phase and a magnetic-only phase, with atomic displacement parameters for the magnetic sites constrained to be equal to those sites in the nuclear phase. A separate peak shape was refined for the magnetic-only phase.

The density functional theory (DFT) calculation was performed on Pb_2NiOsO_6 with the all-electron full-potential linearized augmented plane-wave (FLAPW) method implemented in the WIEN2k code[27]. Generalized gradient approximation (GGA) of Perdew-Burke-Ernzerhof (PBE)[28] was used for the exchange-correlation functional. The spin-orbit coupling was taken into account in the second variation method. To consider the correlation effect, GGA + U was adopted within fully localized limits [29, 30]. The on-site Coulomb interaction parameters U = 4 and 2 eV for Ni and Os, respectively, and the Hund's coupling J_H = 0.8 eV, which was shown to describe the similar compound, Ca_2NiOsO_6 properly[31].

Results

Crystal structure. Room-temperature SPXD data of Pb_2NiOsO_6 were successfully refined in a monoclinic double perovskite structure with space group $P2_1/n$ (see Supporting Information) similar to that reported for Pb_2CoOsO_6[16], Pb_2MnReO_6[32], and

Pb_2CoTeO_6[33]. Due to the weak X-ray scattering power of O (especially in the presence of strong scatterers Os and Pb), complementary neutron powder diffraction (NPD) data were used to confirm this nuclear structure at 98 K. NPD data collected at 98 K (above T_N) are consistent with the SPXD results and can be well fitted with a model of $P2_1/n$ symmetry (see Supporting Information). The Ni and Os ions occupy 2*a* and 2*b* sites, respectively. Allowing for anti-site disorder in the model during the refinement (with constraints to maintain stoichiometry) revealed complete *B*-site ordering (100(6) %). Refinement of the occupancies of Pb and O sites (with a single global atomic displacement parameter) indicated that the material is very close to stoichiometric ($Pb_{1.940(1)}NiOsO_{5.90(1)}$). This stoichiometry was assumed for further analysis. Trace amounts of PbO_2 and NiO impurities were identified and included in the refinement (no Os impurity was detected). Final refined atomic parameters and selected bond lengths and angles are summarized in the Supporting Information. The bond valence sum calculations[34, 35] support the nominal Ni^{2+} and Os^{6+} oxidation states (see Supporting Information). The refined crystal structure is shown in Figure 1a, where the corner-linked NiO_6 and OsO_6 octahedra are ordered in the rock salt manner. The inter-octahedral Ni-O-Os bond angles are 159.20(9)°, 161.3(4)°, and 160.5(4)°, which significantly deviate from 180° and imply substantial rotations of BO_6 octahedra.

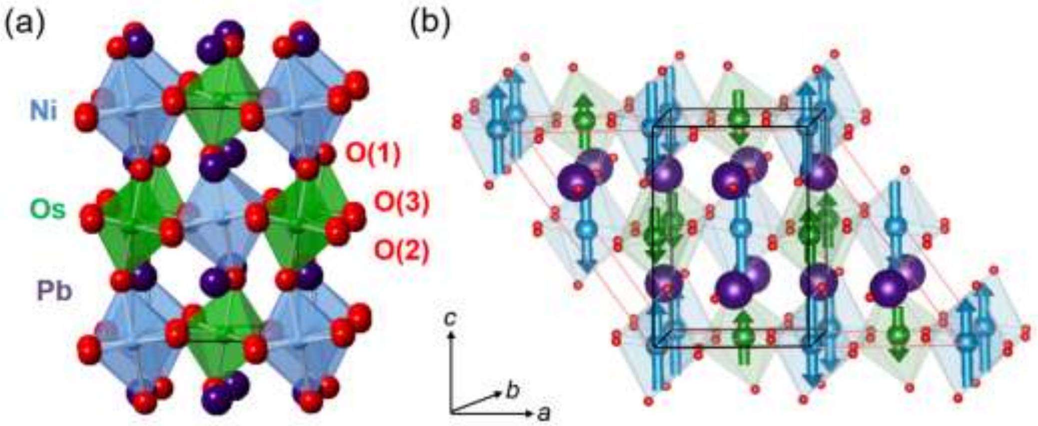

Figure 1 Illustration of the nuclear (a) and magnetic structures (b) of Pb_2NiOsO_6 at 1.5 K from Rietveld refinement using NPD data; Pb, Ni, Os, and O sites are shown in purple, blue, green, and red, respectively; Ni and Os moments are shown by arrows. The nuclear unit cell is shown by solid black lines and the larger, monoclinic P_ac magnetic unit cell by solid red lines.

Electrical and magnetic properties. The temperature dependence of resistivity (ρ) data decreases with cooling as shown in Figure 2a, and shows the metallic nature of Pb_2NiOsO_6. The temperature dependence of magnetic susceptibility (χ) data shows a typical AFM transition with a peak at 58 K (see Figure 2b), which indicates the Néel temperature (T_N). The long-range AFM transition was further confirmed by specific heat data which display a λ-type anomaly at T_N (see Figure 2c). The χ^{-1} vs. T data above the T_N shows the Curie-Weiss behavior. Fitting the CW law to the data between 100 to 380 K results in an effective moment (μ_{eff}) of 3.66 μ_B per formula unit (f.u.) and a Weiss temperature (θ_W) of -102 K. The obtained effective moment is comparable to that in other Ni^{2+}-Os^{6+} double perovskites, 3.44 μ_B/f.u. for Sr_2NiOsO_6[36], and 3.46 μ_B/f.u. for Ba_2NiOsO_6[37]. These values are smaller than the spin-only moments of 4.0 μ_B per formula unit for the Ni^{2+} ($3d^8$: $S = 1$) and Os^{6+} ($5d^2$: $S = 1$), which may be due to the SOC of Os^{6+}. The negative θ_W corroborates that AFM interactions are dominant in Pb_2NiOsO_6, which is consistent with the AFM order. The low-temperature part of specific heat data is plotted in the C_P/T vs. T^2, and the lowest temperature part can be characterized by an approximated Debye model ($C_P/T = \gamma + \beta_0 T^2$). The fitting gives a Sommerfeld coefficient (γ) of 63.5 mJ mol^{-1} K^{-2}. The large γ value is consistent with the metallic nature of Pb_2NiOsO_6. The deviation from linearity above 30 K^2 could be due to the lattice contribution.

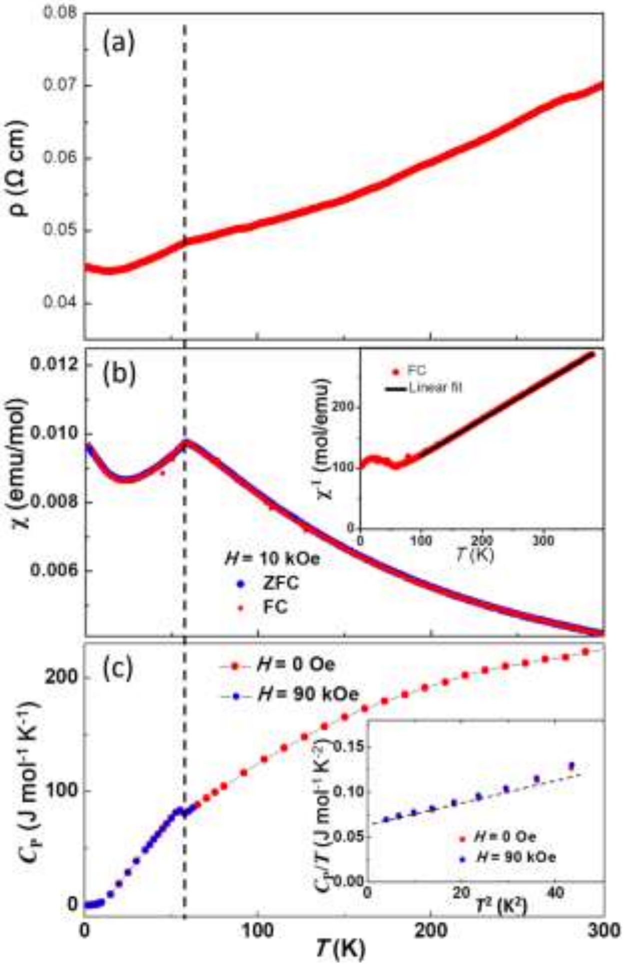

Figure 2 (a) temperature-dependent resistivity, (b) temperature-dependent magnetic susceptibility, and (c) temperature-dependent specific heat of Pb_2NiOsO_6.

Magnetic structure. To study the magnetic structure of Pb_2NiOsO_6, NPD data were collected from 1.5 K to 98 K. On cooling below 57 K, additional reflections were observed in NPD patterns which increased smoothly in intensity on cooling (see Supporting Information). These were consistent with magnetic ordering described by magnetic propagation vector k = (½ 0 ½). As described for the double perovskites Pb_2CoOsO_6[16] and for the k_1 propagation vector for Sc_2NiMnO_6,[38] there are four irreps associated with the magnetic propagation vector k = (½ 0 ½): $mY_1^{\pm}$ and $mY_2^{\pm}$. The mY_n^{+} (mY_n^{-}) irreps describe magnetic order on the Ni (Os) sites only. Magnetic susceptibility and heat capacity measurements for Pb_2NiOsO_6 (Figures 2b and 2c) and the evolution of magnetic Bragg intensity in NPD data collected on cooling (see Supporting Information) suggest a single magnetic ordering transition which could result from one of three possible scenarios: (1) only Ni^{2+} moments order at T_N; (2) only Os^{6+} moments order at T_N or (3), both Ni^{2+} and Os^{6+} moments order simultaneously at T_N. As described for related double perovskites,[36, 38-40] the magnetic moments on the two *B* sites are strongly correlated in refinements and NPD cannot unambiguously distinguish between these three scenarios. However, given the strong coupling between nearest Ni^{2+} and Os^{6+} ions in Ca_2NiOsO_6, it seems most likely that both Ni and Os sublattices order magnetically below T_N.[31] Experiments on Pb_2CoOsO_6 including muon spin rotation experiments support magnetic ordering of both Co^{2+} and Os^{6+} moments[16], consistent with our analysis for Pb_2NiOsO_6. Mode inclusion analysis[41, 42] using 1.5 K data suggested that the greatest improvement in fit was obtained with moments on the Os sites described by mY_2^- (R_{wp} decreased from 7.71% for a non-magnetic model to 6.42% for the mY_2^- model) with Os moments close to [001] direction of the $P2_1/n$ nuclear unit cell. Magnetic ordering described by the mY_2^- irrep on the Os sites and the mY_1^+ (mY_2^+) irrep on the Ni sites breaks inversion symmetry and the ferroelectric mode Γ_2^- (Γ_1^-) is coupled to both magnetic order parameters, allowing polar displacements in the *ac* plane ([010] direction) of the $P2_1/n$ nuclear unit cell. These two possible structures are very similar, and our NPD data do not allow us to confirm which is more appropriate to describe the low temperature nuclear and magnetic structure of Pb_2NiOsO_6. Attempts to investigate the polar distortions using both NPD analysis and electron diffraction were not successful, suggesting that these distortions are very subtle. Consistent with DFT calculations (see below), the mY_2^- mY_1^+ Γ_2^- model was assumed for all further analysis. This magnetic structure is described by the monoclinic unit cell of symmetry P_ac which is related to the $P2_1/n$ nuclear unit cell by the basis vectors (-200) (0-10) (101) with an origin shift of (0 ¼ 0) (see Figure 1b). Given the complexity of the system, the moments on Ni and Os sites were constrained to be collinear (as observed in related systems[16, 31, 34, 38-40, 43]) and the moments on Os sites were constrained to be eight times smaller than those on Ni sites, as might be expected for Ni^{2+} (d^8) and Os^{6+} (d^2) with significantly covalent bonding.[16, 31, 36, 39] Allowing the moment direction to refine freely gave moments close to [001] of the $P2_1/n$ nuclear unit cell and constraining the moments to lie exactly along this direction gave a similar fit (R_{wp} was the same to three decimal places) and was used in subsequent analysis. Allowing atomic displacement parameters (ADPs) to refine anisotropically did not give a significant improvement in fit and ADPs were found to be fairly isotropic. The final refinement profiles and parameters are given in the supporting information.

Sequential Rietveld refinements were carried out using NPD data collected on warming to study the evolution of nuclear and magnetic structures. The 1.5 K model described above was used and this sequential analysis suggested a fairly smooth expansion of the structure on warming (see Supporting Information).

First-principles calculations. Density functional theory (DFT) calculations were carried out to explore whether both Ni and Os moments are ordered in the magnetic phase of Pb_2NiOsO_6, and to differentiate between the possible magnetically ordered structures. Firstly, the total energies were calculated for magnetic models with either AFM order on both Ni and Os sublattices, or AFM order on only the Ni sublattice (see Supporting Information). These calculations indicate that the model with AFM order on both Ni and Os sublattices is 0.102 eV per formula unit more stable than that with only Ni ordered moments. These calculations support the non-centrosymmetric AFM models in which both sublattices are ordered.

As discussed above, group theory calculations assuming the propagation vector (½ 0 ½) and magnetic order on both Ni and Os sublattices (from magnetic irreps mY_1^+ and mY_2^+ on Ni sites, mY_1^- and mY_2^- on Os sites) give four possible isotropy subgroups (Figure 3). These models give comparable fits to the NPD data and we are not able to unambiguously determine the magnetic ground state from our experimental work. Although the relative orientation of magnetic spins is similar in these four structures (they all have the ↑↑↓↓↑↑ sequence of moments on the Ni – Os chains along the [001] direction of the nuclear unit cell), the superposition of the magnetic order on the nuclear structure (with monoclinic symmetry arising from rotations of NiO_6 and OsO_6 octahedra) results in different final symmetries and, as a consequence, in different distortions (e.g. polar degrees of freedom, bond distances and angles) and hence different macroscopic properties.[44-46] Since the four models derive from different combination of irreducible representations these are distinct structures and not translational domains.

DFT calculations were carried out to differentiate between these similar magnetic structures and to determine the ground state. Calculations were carried out using the GGA(PBE)+SOC+U scheme to determine the energy of the four magnetic structures shown in Figure 3 and the relative energies are given in Table 1. Model 2 (described above from analysis of NPD data, Figure 1b) is found to be the lowest in energy for calculations including spin-orbit coupling (Table 1). These results suggest that the ground state of Pb_2NiOsO_6 is best described by P_ac magnetic symmetry, with Γ_2^- polar degrees of freedom, consistent with the ground state reported for Pb_2CoOsO_6[16]. Notice that the same ground state was found for Pb_2NiOsO_6 from calculations without accounting for spin-orbit coupling. Mode decomposition of the relaxed structures from these DFT calculations was carried out using ISODISTORT[26] but the amplitudes of polar displacements were very small (≤0.00035); this is consistent with NPD and electron diffraction analysis both unable to confirm these displacements. The subtlety of these polar distortions (and that they are secondary rather than primary order parmeters) is born out by the fact that the two lowest energy structures (models 1 and 2) allow different polar distortions, suggesting that these distortions play a minor role in giving the non-centrosymmetric ground state structure.

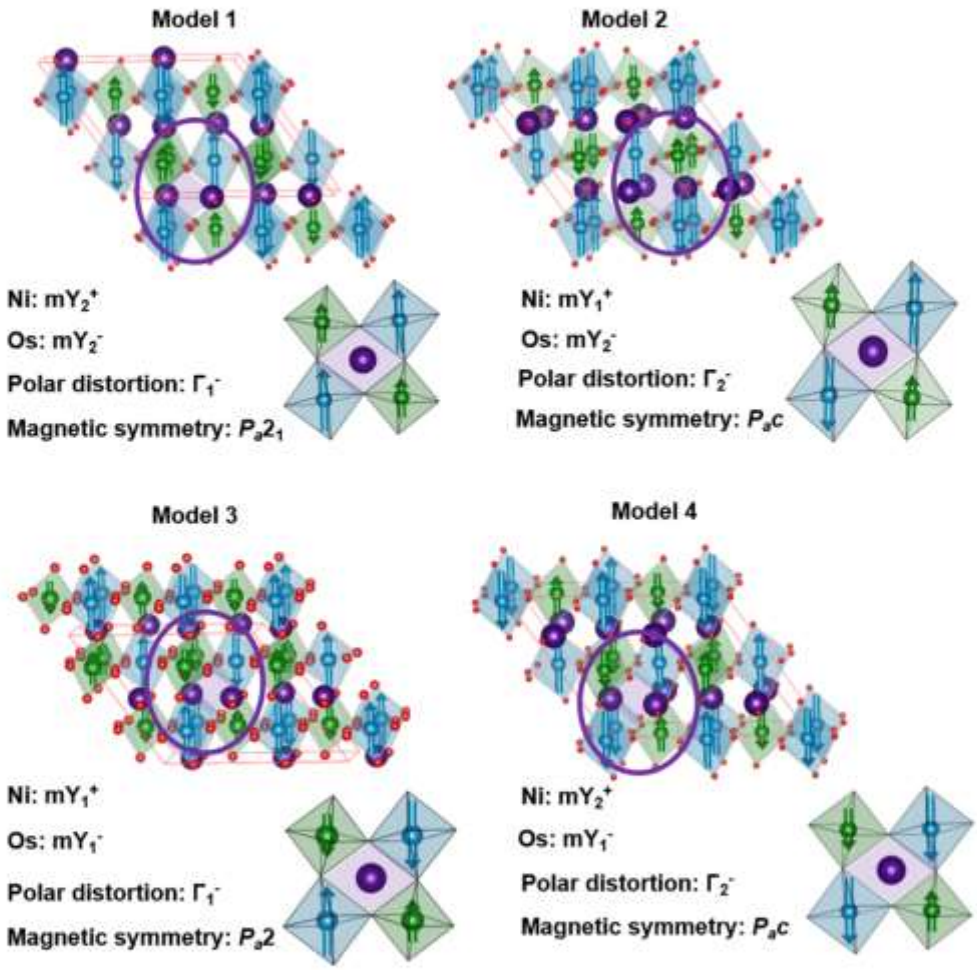

Figure 3 Four magnetic structures that result from the k = (½ 0 ½) magnetic propagation vector for $P2_1/n$ nuclear structure for Pb_2NiOsO_6 with magnetic order on both Ni (blue) and Os (green) sites. To help visualize the difference between the four magnetic structures, the magnetic order around a PbO_{12} site (purple) viewed down the [-1 1 0] direction of the nuclear unit cell is highlighted for each model. (Note that for model 2, the magnetic order around the PbO_{12} site is viewed along [0 -1 0] of the magnetic unit cell to show the magnetic moments about the same point in the nuclear structure.)

Table 1 The total energy and magnetic moment calculated for Pb_2NiOsO_6 for models shown in Figure 3. The unit of the energy is meV per atom and is calculated by dividing the DFT total energy by the number of atoms in the unit cell (40 for the magnetic unit cells shown in Figure 3). Model 1 is chosen as the reference energy. Details about magnetic moments are discussed in the main text.

	Energy (meV/atom)	Total moment (μ_B)	spin moment (μ_B)	orbital moment (μ_B)
Model 1	0	Ni: 1.85 Os: 0.78	Ni: 1.70 Os: 0.99	Ni: 0.15 Os: -0.21
Model 2	**-0.36**	**Ni: 1.86**	**Ni: 1.70**	**Ni: 0.16**

		Os: 0.78	**Os: 0.99**	**Os: -0.21**
Model 3	+0.18	Ni: 1.85 Os: 0.77	Ni: 1.70 Os: 0.99	Ni: 0.15 Os: -0.22
Model 4	+0.42	Ni: 1.85 Os: 0.76	Ni: 1.70 Os: 0.99	Ni: 0.15 Os: -0.23

The electronic structure of Pb_2NiOsO_6 for model 2 (total and partial) is shown in Figure 4. Since Ni and Os atoms have local magnetic moments (Table 1), they show local spin polarization as shown in Figures 4 (b) and (c). These local spin polarizations are summed to be zero, that is, the net total magnetic moment is zero, reflecting that Pb_2NiOsO_6 is antiferromagnetic, as demonstrated in Figure 4 (a).

The major contributions to the total DOS around the E_F are attributed to the Os-5d orbitals in both spin channels, which hybridize strongly with the O-2p orbitals. Occupation numbers for Ni 3d and Os 5d are 7.81 and 3.80, respectively. The huge hybridization indicated between Os 5d and O 2p orbitals suggests Ni^{2+} and Os^{6+} formal oxidation states in Pb_2NiOsO_6, consistent with the magnetic susceptibility experiment. Spin and orbital moments for Ni are 1.70 and 0.16 μ_B, respectively, thereby giving a total magnetic moment of 1.86 μ_B per Ni. For Os, spin and orbital moments are 0.99 and -0.21 μ_B respectively, where the minus sign indicates that the orbital moment is opposite the spin direction, thus the total moment is 0.78 μ_B per Os. These calculated moments are comparable with those obtained from NPD analysis (see above). The calculated γ is 7.1 mJ mol^{-1} K^{-2}. This is much smaller than the one obtained from the fitting of low-temperature specific heat data (63.5 mJ mol^{-1} K^{-2}), which may be due to the fact that DFT underestimates the electronic correlations in the correlated systems, resulting in a relatively small gamma value.

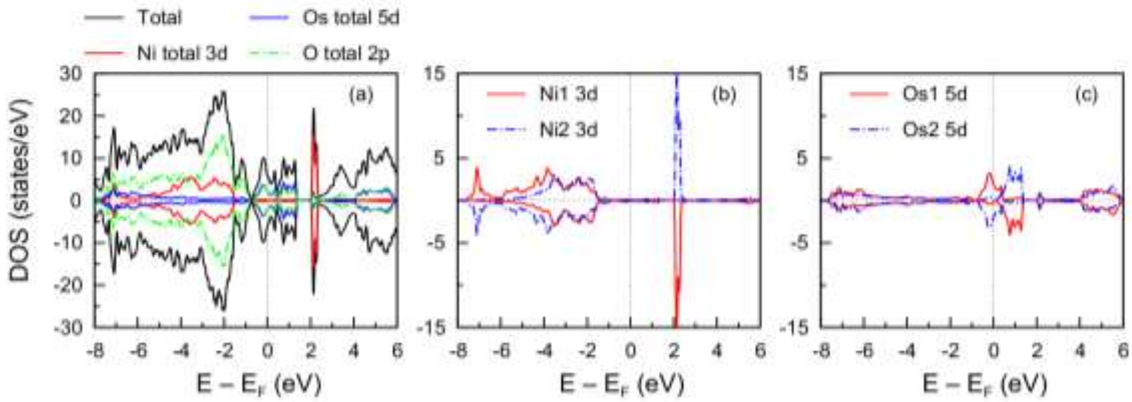

Figure 4 Total and partial density of states (DOS) of Pb_2NiOsO_6 for model 2 from GGA+SOC+U calculation. (a) The black solid line corresponds to the total DOS. Red solid, blue solid, and green dash-dotted lines represent total Ni 3d, total Os 5d, and O 2p partial DOS, respectively. (b) Partial DOS for each Ni 3d: Ni1 (Ni2) is presented for the spin majority as spin up (down). (c) Partial DOS for each Os 5d: Os1 (Os2) is presented for the spin majority as spin up (down). The positive and negative values in DOS correspond to spin up and down, respectively.

Discussion

The A_2NiOsO_6 (A = Ca^{2+}, Sr^{2+}, Ba^{2+} and now Pb^{2+}) oxides adopt *B*-site ordered double perovskite structures and span a range of properties, from insulating (A = Ca[31]) to metallic (A = Pb), and from ferromagnetic (A = Ba at low temperatures[37]) to antiferromagnetic (A = Sr[36]). While all these analogs adopt the rock-salt ordering of NiO_6 and OsO_6 octahedra, the degree of tilting of these octahedra increases with decreasing *A* cation radius: Ba_2NiOsO_6 is cubic with 180° Ni – O – Os bond angles; in tetragonal Sr_2NiOsO_6, octahedra are tilted about the long axis giving 180°/166° Ni – O – Os angles[36], while Ca_2NiOsO_6 adopts the monoclinic $P2_1/n$ structure (with $a^-a^-c^+$ tilts) with Ni – O – Os angles of ~151°.[36] Pb_2NiOsO_6 also adopts this $P2_1/n$ structure despite the ionic radius of Pb^{2+} (1.49 Å) being comparable to that of Sr^{2+} (1.44 Å)[47]; this might in part be due to the inert pair Pb^{2+} ion favoring the lower symmetry coordination environment[48] possible in the $P2_1/n$ structure: Pb occupies the 4*e* site of 1 symmetry in $P2_1/n$ compared with the higher symmetry 4*d* site of -4.. symmetry in the $I4/m$ structure of Sr_2NiOsO_6.

The magnetic structure described here for Pb_2NiOsO_6 is of the same symmetry as that reported for Pb_2CoOsO_6[16], although with a slightly different orientation of moments, likely resulting from the different magnetic anisotropies of Co^{2+} and Ni^{2+} ions in octahedral coordination environments. In both Pb_2NiOsO_6 and Pb_2CoOsO_6, the magnetic order on the Ni/Co and Os sublattices breaks inversion symmetry and follows an ↑↑↓↓ sequence along [001] of the nuclear unit cell. Magnetic ordering has been shown to break inversion symmetry in other perovskites, including Sr_2NiMnO_6, but with weak coupling between Ni and Mn sublattices,[38] in contrast to $Pb_2\textit{B}OsO_6$ (B = Co, Ni) which seem to have collinear moments on both B and Os sublattices and a single magnetic ordering transition. These observations are consistent with strong couplings between Co/Ni and Os sublattices. This ↑↑↓↓ magnetic structure observed in Pb_2NiOsO_6 is significantly different to those reported for other A_2NiOsO_6 double perovskites. Previous work has highlighted the importance of both nearest-neighbor (likely FM) and next-nearest-neighbor (likely AFM) interactions in these systems.[31, 49] The balance between these (competing) interactions gives some magnetic frustration in Sr_2NiOsO_6 and makes the magnetic structure of A_2NiOsO_6 phases very sensitive to bond angles.[31]

The symmetry requirements for magnetic order to break inversion symmetry have been explored by Perez-Mato et al[50] and provide a recipe for designing new magnetoelectrics. If the magnetic k vector is not compatible with the screw axes or glide planes of the nuclear (paramagnetic) unit cell (when time reversal symmetry is considered), then full magnetic order on a lattice of magnetic atoms on special sites (of -1 symmetry) will break inversion symmetry, resulting in non-centrosymmetric structures.[50]

The double perovskites considered here have rocksalt ordering of B and B' cations on sites related by an origin shift (and typically with symmetries including inversion centers). If a single magnetic propagation vector k describes the magnetically ordered phase, and full magnetic order is expected on both B and B' sublattices, then depending on k, the irreps to describe the magnetic order on each sublattice may be of opposite parity with respect to an inversion centre at the origin. These irreps couple to a non-centrosymmetric distortion (Γ_x^-), breaking inversion symmetry. This is the case described here for Pb_2NiOsO_6 for k = (½ 0 ½) and also for k = (-1 ½ ½). Likewise for a cubic double perovskite $A_2BB'O_6$ of *Fm*-3*m* nuclear symmetry (with magnetic *B* and *B'* ions on 4*a* and 4*b* sites, respectively), a magnetic k = (½ ½ ½) would have a similar effect. This is also observed in the hexagonal Ca_3CoMnO_6 (*R*-3*c* nuclear symmetry, Mn^{3+} and Co^{3+} ions on 6*a* (0 0 ¼) and 6*b* (0 0 0) sites respectively) with magnetic k = (0 0 0) giving the well-known ↑↑↓↓ polar magnetic structure.[51]

If suitable cation ordered structures with strong magnetic coupling between the two sublattices (to favor them ordering with the same magnetic k vector) can be identified, then new magnetoelectrics might be designed if the magnetic exchange interactions can be balanced to give the desired k vector. We note that the improper ferroelectricity described here does not require additional ordering of *A*-site cations (e.g. the *AA'*$NiOsO_6$ phases explored recently).[52]

It is striking that both Pb_2NiOsO_6 and Pb_2CoOsO_6[16] are metallic, in contrast to the SOC Mott-insulating nature of Ca_2NiOsO_6 and Ca_2CoOsO_6,[31] despite the structural similarities between these Pb and Ca analogs. Firstly, we note that although Pb_2NiOsO_6 is metallic, its resistivity is several orders of magnitude higher than that of Pb_2CoOsO_6 (300 K resistivity is ~0.07 Ω cm (Figure 2a) and ~3.5×10^{-4} Ω cm for Ni and Co[16] analogs, respectively). This is similarly observed for Ca_2NiOsO_6 and Ca_2CoOsO_6 and is ascribed to the full occupancy of the Ni^{2+} t_{2g} band reducing delocalization of Os^{6+} t_{2g} electrons.[31]

The half-metallic nature proposed for Sr_2NiOsO_6 results from the partially-occupied Os t_{2g} states crossing the Fermi level, with spin-orbit coupling broadening the Os 5d bands.[53] This scenario can be applied to A_2NiOsO_6 (*A* = Ca, Pb) and our PDOS calculations (Figure 4) are qualitatively similar to those reported for Ca_2NiOsO_6 [31] (with Ni t_{2g} states below ~-2eV and a narrow band of Ni e_g states at ~2 eV, with Os 5d and O 2p bands crossing E_F). However, the bandwidth in these double perovskites is also influenced by Ni – O – Os bond angles: in Ca_2NiOsO_6 with small Ca^{2+} ions, the Ni – O – Os angles (~149.3-150.6° at 4 K)[36] show much larger deviations from the ideal 180° bond angles than in Pb_2NiOsO_6 (158.8-161.0° at 1.5 K). The more distorted structure reported for the Ca analogs is likely to decrease the orbital overlap and bandwidth, giving wider band gaps than the less distorted Pb analogs. This is consistent with the insulating and more localized nature of Ca_2NiOsO_6 and its higher magnetic ordering temperature (158 K, compared with T_N = 58 K for Pb_2NiOsO_6).

Conclusion

A new 5d oxide Pb_2NiOsO_6 was synthesized under high-pressure. Pb_2NiOsO_6 crystallizes in a monoclinic double perovskite structure with a centrosymmetric space group $P2_1/n$ at room temperature. Pb_2NiOsO_6 is metallic down to 2 K and displays an AFM transition with T_N = 58 K. Pb_2NiOsO_6 is a new example of AFM metallic oxide with three-dimensional crystal and electronic structures. NPD and DFT calculations indicate that both the Ni and Os moments are ordered below T_N, breaking inversion symmetry, which is similar to recently-reported Pb_2CoOsO_6[16, 17]. The magnetically driven loss of center of symmetry is similar to the type-II multiferroics. The discovery of 5d oxides Pb_2NiOsO_6 together with Pb_2CoOsO_6 establishes a new class of noncentrosymmetric AFM metallic oxides.

Acknowledgment

C.-J.K. and G.K. were supported by the National Science Foundation Grant No. DMR1733071. MG was supported by the Center for Computational Design of Functional Strongly Correlated Materials and Theoretical Spectroscopy under DOE Grant No. DE-FOA-0001276. This study was supported in part by JSPS KAKENHI Grants No. JP20H05276, a research grant from Nippon Sheet Glass Foundation for Materials Science and Engineering (Grant No. 40-37), and Innovative Science and Technology Initiative for Security (Grant No. JPJ004596) from Acquisition, Technology & Logistics Agency (ATLA), Japan. We're grateful to the ISIS Neutron and Muon Source (S.T.F.C., U.K.) for the provision of neutron diffraction beamtime.[54]

ASSOCIATED CONTENT

Supporting Information

Supplemental data: Refined room-temperature SXRD pattern and the corresponding crystal structure information. Refined PND data at 98 and 1.5 K and the corresponding crystal structure information. Evolution of nuclear and magnetic structures with temperature for Pb_2NiOsO_6 from sequential refinements using NPD data. DFT calculations of Pb_2NiOsO_6 with the different magnetic states.

References

1. Goodenough, J. B. Magnetism and the Chemical Bond (Interscience publisher, New York-London, 1963).

2. Komarek, A. C.; Streltsov, S. V.; Isobe, M.; Moller, T.; Hoelzel, M.; Senyshyn, A.; Trots, D.; Fernandez-Diaz, M. T.; Hansen, T.; Gotou, H.; Yagi, T.; Ueda, Y.; Anisimov, V. I.; Grueninger, M.; Khomskii, D. I.; Braden, M. $CaCrO_3$: An Anomalous Antiferromagnetic Metallic Oxide. *Phys. Rev. Lett.* **2008,** *101*, 167204.

3. Cava, R. J.; Batlogg, B.; Krajewski, J. J.; Gammel, P.; Poulsen, H. F. Antiferromagnetism and Metallic Conductivity in $Nb_{12}O_{29}$. *Nature* **1991**, *350*, 598-600.

4. Cheng, J.-G.; Zhou, J.-S.; Goodenough, J. B.; Zhou, H. D.; Wiebe, C. R.; Takami, T.; Fuji, T. Spin Fluctuations in the Antiferromagnetic metal $Nb_{12}O_{29}$. *Phys. Rev. B* **2009**, *80*, 134428.

5. Argyriou, D. N.; Mitchell, J. F.; Radaelli, P. G.; Bordallo, H. N.; Cox, D. E.; Medarde, M.; Jorgensen, J. D. Lattice Effects and Magnetic Structure in the Layered Colossal Magnetoresistance Manganite $La_{2-2x}Sr_{1+2x}Mn_2O_7$, x = 0.3. *Phys. Rev. B* **1999,** *59*, 8695-8702.

6. Yoshida, Y.; Ikeda, S. I.; Matsuhata, H.; Shirakawa, N.; Lee, C. H.; Katano, S. Crystal and Magnetic Structure of $Ca_3Ru_2O_7$. *Phys. Rev. B* **2005,** *72*, 054412.

7. Berlijn, T.; Snijders, P. C.; Delaire, O.; Zhou, H. D.; Maier, T. A.; Cao, H. B.; Chi, S. X.; Matsuda, M.; Wang, Y.; Koehler, M. R.; Kent, P. R. C.; Weitering, H. H. Itinerant Antiferromagnetism in RuO_2. *Phys. Rev. Lett.* **2017,** *118*, 077201.

8. Zhu, Z. H.; Strempfer, J.; Rao, R. R.; Occhialini, C. A.; Pelliciari, J.; Choi, Y.; Kawaguchi, T.; You, H.; Mitchell, J. F.; Shao-Horn, Y.; Comin, R. Anomalous Antiferromagnetism in Metallic RuO_2 Determined by Resonant X-Ray Scattering. *Phys. Rev. Lett.* **2019,** *122*, 017202.

9. Guo, H.; Li, Z. W.; Zhao, L.; Hu, Z.; Chang, C. F.; Kuo, C. Y.; Schmidt, W.; Piovano, A.; Pi, T. W.; Sobolev, O.; Khomskii, D. I.; Tjeng, L. H.; Komarek, A. C. Antiferromagnetic Correlations in the Metallic Strongly Correlated Transition Metal Oxide $LaNiO_3$. *Nat Commun* **2018,** *9*, 43.

10. Witczak-Krempa, W.; Chen, G.; Kim, Y. B.; Balents, L. Correlated Quantum Phenomena in the Strong Spin-Orbit Regime. *Annu. Rev. Conden. Matter Phys.* **2014,** *5*, 57-82.

11. Jackbsen, H.; Feng, H. L.; Princep, A. J.; Rahn, M. C.; Guo, Y.; Chen, J.; Matsushita, Y.; Tsujimoto, Y.; Nagao, M.; Khalyavin, D.; Manuel, P.; Murray, C. A.; Donnerer, C.; Vale, J. G.; Sala, M. M.; Yamaura, K.; Boothroyd, A. T. Magnetically Induced Metal-Insulator Transition in Pb_2CaOsO_6. *Phys. Rev. B* **2020,** *102*, 214409.

12. Mandrus, D.; Thompson, J. R.; Gaal, R.; Forro, L.; Brayan, J. C.; Chakoumakos, B. C.; Woods, L. M.; Sales, B. C.; Fishman, R. S.; Keppns, V. Continuous Metal-Insulator Transition in the Pyrochlore $Cd_2Os_2O_7$. *Phys. Rev. B* **2001,** *63*, 195104.

13. Padilla, W. J.; Mandrus, D.; Basov, D. N. Searching for the Slater Transition in the Pyrochlore $Cd_2Os_2O_7$ with Infrared Spectroscopy. *Phys. Rev. B* **2005,** *66*, 035120.

14. Calder, S.; Garlea, V. O.; McMorrow, D. F.; Lumsden, M. D.; Stone, M. B.; Lang, J. C.; Kim, J.-W.; Schueter, J. A.; Shi, Y. G.; Yamaura, K.; Sun, Y. S.; Tsujimoto, Y.; Christianson, A. D. Magnetically Driven Metal-Insulator Transition in $NaOsO_3$. *Phys. Rev. Lett.* **2012,** *108*, 257209.

15. Shi, Y. G.; Guo, Y.; Wang, X.; Princep, A. J.; Khalyavin, D.; Manuel, P.; Michiue, Y.;

Sato, A.; Tsuda, K.; Yu, S.; Arai, M.; Shirako, Y.; Akaogi, M.; Wang, N.; Yamaura, K.; Boothroyd, A. T. A Ferroelectric-like Structural Transition in a Metal. *Nat. Mater.* **2013,** *12*, 1024–1027.

16. Princep, A. J.; Feng, H. L.; Guo, Y. F.; Lang, F.; Weng, H. M.; Manuel, P.; Khalyavin, D.; Senyshyn, A.; Rahn, M. C.; Yuan, Y. H.; Matsushita, Y.; Blundell, S. J.; Yamaura, K.; Boothroyd, A. T. Magnetically Driven Loss of Centrosymmetry in Metallic Pb_2CoOsO_6. *Phys. Rev. B* **2020,** *102*, 104410.

17. Jiao, Y.; Fang, Y.-W.; Sun, J.; Shan, P.; Yu, Z.; Feng, H. L.; Wang, B.; Ma, H.; Uwatoko, Y.; Yamaura, K.; Guo, Y.; Chen, H.; Cheng, J. Coupled Magnetic and Structural Phase Transitions in the Antiferromagnetic Polar Metal Pb_2CoOsO_6 Under Pressure. *Phys. Rev. B* **2020**, *102*, 144418.

18. Yamaura, K. Short Review of High-Pressure Crystal Growth and Magnetic and Electrical Properties of Solid-State Osmium Oxides. *J. Solid State Chem.* **2016,** *236*, 45-54.

19. Tanaka, M.; Katsuya, Y.; Matsushita, Y.; Sakata, O. Development of a Synchrotron Powder Diffractometer with a One-Dimensional X-Ray Detector for Analysis of Advanced Materials. *J. Ceram. Soc. Jpn* **2013,** *121*, 287-290.

20. Tanaka, M.; Katsuya, Y.; Yamamoto, A. A New Large Radius Imaging Plate Camera for High-Resolution and High-Throughput Synchrotron X-Ray Powder Diffraction by Multiexposure Method. *Rev. Sci. Instru.* **2008,** *79*, 075106.

21. Izumi, F.; Ikeda, T. A Rietveld-Analysis Programm RIETAN-98 and its Applications to Zeolite. *Mater. Sci. Forum* **2000,** *321-324*, 198-205.

22. Momma, K.; Izumi, F. VESTA 3 for Three-Dimensional Visualization of Crystal, Volumetric and Morphology data. *J. Appl. Crystallogr.* **2011,** *44*, 1272-1276.

23. Chapon, L. C.; Manuel, P.; Radaelli, P. G.; Benson, C.; Perrott, L.; Ansell, S.; Rhodes, N. J.; Raspino, D.; Duxbury, D.; Spill, E.; Norris, J. Wish: The New Powder and Single Crystal Magnetic Diffractometer on the Second Target Station. *Neutron News* **2011,** *22*, 22-25.

24. Coelho, A. A. Indexing of Powder Diffraction Patterns by Iterative Use of Singular Value Decomposition. *J. Appl. Cryst.* **2003,** *36*, 86-95.

25. Coelho, A. A. Topas Academic: General Profile and Structure Analysis Software for Powder Diffraction Data. Bruker AXS: Karlsruhe, Germany, 2012.

26. Campbell, B. J.; Stokes, H. T.; Tanner, D. E.; Hatch, D. M. ISODISTORT. *J. Appl. Cryst.* **2006,** *39*, 607-614.

27. Blaha, P.; Schwarz, K.; Madsen, G. K. H.; Kvasnicka, D.; Luitz, J. WIEN2K, an Augmented Plane Wave + Local Orbitals Program for Calculating Crystal Properties. *Technische Universitët Wien: Wien, Austria, 2001.*

28. Perdew, J. P.; Burke, K.; Ernzerhof, M. Generalized Gradient Approximation Made Simple. *Phys. Rev. Lett.* **1996,** *77*, 3865-3868.

29. Anisimov, V. I.; Solovyev, I. V.; Korotin, M. A.; Czyzyk, M. T.; Sawatzky, G. A. Density-Functional Theory and Nio Photoemission Spectra. *Phys. Rev. B* **1993,** *48*, 16929-16934.

30. Anisimov, V. I.; Aryasetiawan, F.; Lichtenstein, A. I. First-Principles Calculations of the Electronic Structure and Spectra of Strongly Correlated Systems: The LDA+U Method. *J. Phys.:Condens. Matter* **1997,** *9*, 767-808.

31. Morrow, R.; Samanta, K.; Dasgupta, T. S.; Xiong, J.; Freeland, J. W.; Haskel, D.; Woodward, P. M. Magnetism in Ca_2CoOsO_6 and Ca_2NiOsO_6: Unraveling the Mystery of Superexchange Interactions between 3d and 5d Ions. *Chem. Mater.* **2016,** *28*, 3666-3675.

32. Ramesha, K.; Sebastian, L.; Eichhorn, B.; Gopalakrishnan, J. Perovskite and Pyrochlore

Modifications of Pb_2MnReO_6: Synthesis, Structure, and Electronic Properties. *Chem. Mater.* **2003,** *15*, 668-674.

33. Ivanov, S. A.; Nordblad, P.; Mathieu, R.; Tellgren, R.; Ritter, C., Structural and Magnetic Properties of the Ordered Perovskite Pb_2CoTeO_6. *Dalton T* **2010,** *39*, 11136-11148.

34. Brown, I. D.; Altermatt, D. Bond-Valence Parameters Obtained From a Systematic Analysis of the Inorganic Crystal-Structure Database. *Acta Crystallographica Section B-Structural Science* **1985,** *41*, 244-247.

35. Brese, N. E.; Okeeffe, M. Bond-Valence Parameters for Solids. *Acta Crystallographica Section B-Structural Science* **1991,** *47*, 192-197.

36. Macquart, R.; Kim, S. J.; Gemmill, W. R.; Stalick, J. K.; Lee, Y.; Vogt, T.; zur Loye, H. C. Synthesis, Structure, and Magnetic Properties of Sr_2NiOsO_6 and Ca_2NiOsO_6: Two New Osmium-Containing Double Perovskites. *Inorg. Chem.* **2005,** *44*, 9676-9683.

37. Feng, H. L.; Calder, S.; Ghimire, M. P.; Yuan, Y. H.; Shirako, Y.; Tsujimoto, Y.; Matsushita, Y.; Hu, Z. W.; Kuo, C. Y.; Tjeng, L. H.; Pi, T. W.; Soo, Y. L.; He, J. F.; Tanaka, M.; Katsuya, Y.; Richter, M.; Yamaura, K. Ba_2NiOsO_6: A Dirac-Mott Insulator with Ferromagnetism Near 100 K. *Phys. Rev. B* **2016,** *94*, 235158.

38. Yi, W.; Princep, A. J.; Guo, Y.; Johnson, R. D.; Khalyavin, D.; Manuel, P.; Senshyn, A.; Presniakov, I. A.; Sobolev, A. V.; Matsushita, Y.; Tanaka, M.; Belik, A. A.; Boothroyd, A. T. Sc_2NiMnO_6: a Double Perovskite with Magnetoelectric Response Driven by Multiple Magentic Orders. *Inorg. Chem.* **2015,** *54*, 8012-8021.

39. Morrow, R.; Yan, J.; McGuire, M. A.; Freeland, J. W.; Haskel, D.; Woodward, P. M. Effects of Chemical Pressure on the Magnetic Ground States of the Osmate Double Perovskites $SrCaCoOsO_6$ and Ca_2CoOsO_6. *Phys. Rev. B* **2015,** *92*, 094435.

40. Morrow, R.; Freeland, J. W.; Woodward, P. M. Probing the Links between Structure and Magnetism in $Sr_{2-x}Ca_xFeOsO_6$ Double Perovskites. *Inorg. Chem.* **2014,** *53*, 7983-7992.

41. Tuxworth, A. J.; McCabe, E. E.; Free, D. G.; Clark, S. J.; Evans, J. S. O. Structural Characterization and Physical Properties of the New Transition Metal Oxyselenide $La_2O_2ZnSe_2$. *Inorg. Chem.* **2013,** *52*, 2078-2085.

42. McCabe, E. E.; Stock, C.; Rodrigues, E. E.; Wills, A. S.; Taylor, J. W.; Evans, J. S. O. Weak Spin Interactions in Mott Insulating $La_2O_2Fe_2OSe_2$. *Phys. Rev. B* **2014,** *89*, 100402(R).

43. Taylor, A. E.; Morrow, R.; Lumsden, M. D.; Calder, S.; Upton, M. H.; Kolesnikov, A. I.; Stone, M. B.; Fishman, R. S.; Paramekanti, A.; Woodward, P. M.; Christianson, A. D. Origin of Magnetic Excitation Gap in Double Perovskite Sr_2FeOsO_6. *Phys. Rev. B* **2018,** *98*, 214422.

44. Khalyavin, D. D.; Salak, A. N.; Olekhnovich, N. M.; Pushkarev, A. V.; Radyush, Y. V.; Manuel, P.; Raevski, I. P.; Zheludkevich, M. L.; Ferreira, M. G. S. Polar and Antipolar Polymorphs of Metastable Perovskite $BiFe_{0.5}Sc_{0.5}O_3$. *Phys. Rev. B* **2014,** *89*, 174414.

45. Prosandeev, S. A.; Khalyavin, D. D.; Raevski, I. P.; Salak, A. N.; Olekhnovich, N. M.; Pushkarev, A. V.; Radyush, Y. V. Complex Antipolar 2×4×22 Structure with Pnma Symmetry in $BiFeO_3$ and $BiFe_{1/2}Sc_{1/2}O_3$: First-Principles Calculations. *Phys. Rev. B* **2014,** *90*, 054110.

46. Schoop, L. M.; Topp, A.; Lippmann, J.; Orlandi, F.; Müchler, L.; Vergniory, M. G.; Sun, Y.; Rost, A. W.; Duppel, V.; Krivenkov, M.; Sheoran, S.; Manuel, P.; Varykhalov, A.; Yan, B.; Kremer, R. K.; Ast, C. R.; Lotsch, B. V. Tunable Weyl and Dirac States in the Nonsymmorphic Compound CeSbTe. *Science Advances* **2018,** *4*, eaar2317.

47. Shannon, R. Revised Effective Ionic Radii and Systematic Studies of Interatomic Distances in

Halides and Chalcogenides. *Acta Crystallographica Section A* **1976,** *32*, 751-767.
48. Walsh, A.; Payne, D. J.; Egdell, R. G.; Watson, G. W. Stereochemistry of Post-Transition Metal Oxides: Revision of the Classical Lone Pair Model. *Chem. Soc. Rev.* **2011,** *40*, 4455-4463.
49. Tian, C.; Wibowo, A. C.; zur Loye, H.-C.; Whangbo, M.-H. On the Magnetic Insulating States, Spin Frustration, and Dominant Spin Exchange of the Ordered Double-Perovskites Sr_2CuOsO_6 and Sr_2NiOsO_6: Density Functional Analysis. *Inorg Chem* **2011,** *50* (9), 4142-4148.
50. Perez-Mato, J. M.; Gallego, S. V.; Elcoro, L.; Tasci, E.; Aroyo, M. I. Symmetry Conditions for Type II Multiferroicity in Commensurate Magnetic Structures. *J. Phys.:Condens. Matter* **2016,** *28*, 286001.
51. Choi, Y. J.; Yi, H. T.; Lee, S.; Huang, Q.; Kiryukhin, V.; Cheong, S.-W. Ferroelectricity in an Ising Chain Magnet. *Phys. Rev. Lett.* **2008,** *100*, 047601.
52. Shaikh, M.; Fathima, A.; Swamynadhan, M. J.; Das, H.; Ghosh, S. Investigation into Cation-Ordered Magnetic Polar Double Perovskite Oxides. *Chem. Mater.* **2021,** *33*, 1594-1606.
53. Ghimire, M. P.; Hu, X., Compensated Half Metallicity in Osmium Double Perovskite Driven by Doping Effects. *Mater. Res. Express* **2016,** *3*, 106107.
54. Gong, S.; Guo, S.-D.; Chen, P.; Liu, B.-G. Oxygen-Octahedral Distortion and Electronic Correlation Induced Semiconductor Gaps in Ferrimagnetic Double Perovskite Ca_2MReO_6 (M = Cr, Fe). *RSC Adv.* **2015,** *5*, 63165-63174.

TOC graphic

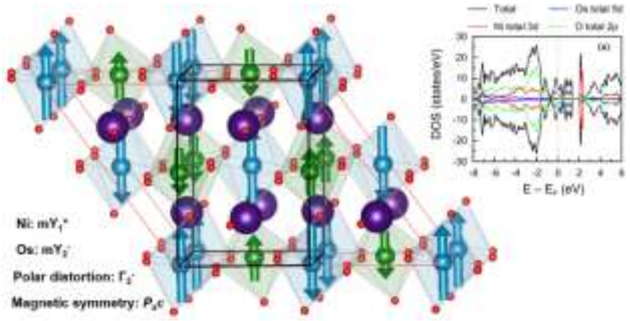

Total
Os total 5d
Ni total 3d
O total 2p
(a)
DOS (states/eV)
E – E_F (eV)
Ni: mY1+
Os: mY2-
Polar distortion: Γ2-
Magnetic symmetry: Pac

Supplementary material

Antiferromagnetic order breaks inversion symmetry in metallic double perovskite, Pb_2NiOsO_6

Hai L. Feng,[1,2] Chang-Jong Kang,[3,4] Pascal Manuel,[5] Fabio Orlandi,[5] Yu Su,[6,7] Jie Chen,[6,7] Yoshihiro Tsujimoto,[6,7] Joke Hadermann,[8] Gabriel Kotliar,[3] Kazunari Yamaura,[6,7] Emma E. McCabe,[9, 10*] Martha Greenblatt[1*]

[1]Department of Chemistry and Chemical Biology, Rutgers, the State University of New Jersey, 123 Bevier Road, Piscataway, NJ 08854, USA

[2]Beijing National Laboratory for Condensed Matter Physics and Institute of Physics, Chinese Academy of Sciences, Beijing 100190, China

[3]Department of Physics and Astronomy, Rutgers, the State University of New Jersey, 136 Frelinghuysen Road, Piscataway, NJ 08854, USA

[4]Department of Physics, Chungnam National University, Daejeon 34134, South Korea

[5]ISIS facility, STFC, Rutherford Appleton Laboratory, Chilton, Didcot, Oxfordshire OX11 0QX, UK.

[6]International Center for Materials Nanoarchitectonics (WPI-MANA), National Institute for Materials Science, Tsukuba, Ibaraki 305-0044, Japan

[7]Graduate School of Chemical Sciences and Engineering, Hokkaido University, Sapporo, Hokkaido 060-0810, Japan

[8]EMAT, University of Antwerp, Groenenborgerlaan 171, 2020 Antwerp, Belgium

[9]School of Physical Sciences, University of Kent, Canterbury, Kent CT2 7NH, UK

[10]Department of Physics, Durham University, Lower Mountjoy, South Road, Durham, DH1 3LE, UK

*Martha Greenblatt
greenbla@chem.rutgers.edu

*Emma E. McCabe
emma.mccabe@durham.ac.uk

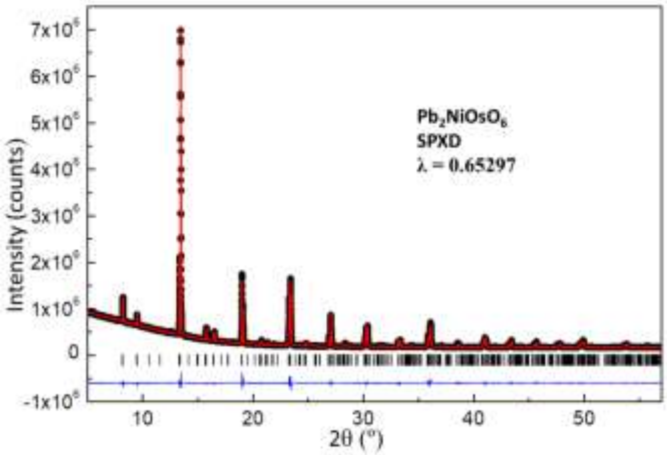

Figure S1 Rietveld refined room temperature SPXD pattern of Pb_2NiOsO_6. Black dots and red solid lines show the observed and calculated patterns, respectively. The difference between the observed and calculated patterns is shown as blue lines at the bottom. The vertical bars indicate positions of expected Bragg reflections for the titled compound.

Table S1 Atomic positions and isotropic displacement factors obtained from the SPXD data of Pb_2NiOsO_6*

Atom	Site	*x*	*y*	*z*	B_{iso} (Å^2)
Pb	4*e*	0.5022(8)	0.5062(4)	0.2503(1)	1.20(1)
Ni	2*c*	0.0	0.5	0.0	0.26(1)
Os	2*b*	0.5	0.0	0.0	0.26(1)
O1	4*e*	0.254(10)	0.248(7)	1.00(3)	1.0(fixed)
O2	4*e*	0.260 (10)	0.740(7)	1.00(3)	1.0(fixed)
O3	4*e*	0.428 (3)	0.927 (2)	0.221(2)	1.0(fixed)

*Space group $P2_1/n$: *a*=5.58724(3) Å, *b*=5.62988(2) Å, *c*=7.89791(3) Å, β = 90.001 (6)°; R_{wp}=2.16, R_p=1.16.

Table S2 Selected bond distances and bond angles for Pb_2NiOsO_6 refined from SPXD and NPD data at different temperatures.

Temperature	298 K	98 K	1.5 K
Diffraction source	Synchrotron	Neutron	Neutron
Pb – O(1)	1 × 2.82(17) Å	1 × 2.470(2) Å	1 × 2.464(2)
Pb – O(1)	1 × 2.79(18) Å	1 × 2.945(3) Å	1 × 2.960(2)
Pb – O(1)	1 × 2.81(17) Å	1 × 2.679(3) Å	1 × 2.666(2)
Pb – O(1)	1 × 2.77(18) Å	1 × 3.153(2) Å	1 × 3.155(2)
Pb – O(2)	1 × 2.88(17) Å	1 × 2.499(7) Å	1 × 2.487(7)
Pb – O(2)	1 × 2.73(18) Å	1 × 2.820(8) Å	1 × 2.803(8)
Pb – O(2)	1 × 2.76(18) Å	1 × 2.724(7) Å	1 × 2.725(7)
Pb – O(2)	1 × 2.83(17) Å	1 × 3.163(7) Å	1 × 3.183(7)
Pb – O(3)	1 × 2.455(18) Å	1 × 2.491(7) Å	1 × 2.495(7)
Pb – O(3)	1 × 3.296(11) Å	1 × 2.812(8) Å	1 × 2.819(8)
Pb – O(3)	1 × 2.415(11) Å	1 × 2.732(7) Å	1 × 2.715(7)
Pb – O(3)	1 × 3.223(18) Å	1 × 3.176(7) Å	1 × 3.179(7)
Ni – O(1)	2 ×2.01(5) Å	2 × 2.091(6) Å	2 × 2.090(6)
Ni – O(2)	2 ×1.98(5) Å	2 × 2.079(5) Å	2 × 2.067(5)
Ni – O(3)	2 ×2.275(13) Å	2 × 2.084(4) Å	2 × 2.074(5)
Os – O(1)	2 ×1.95(5) Å	2 × 1.910(6) Å	2 × 1.914(5)
Os – O(2)	2 ×1.99(5) Å	2 × 1.935(5) Å	2 × 1.941(5)
Os – O(3)	2 ×1.841(13) Å	2 × 1.933(4) Å	2 × 1.940(5)
Os – O(1) – Ni	179.5(12) °	159.20(9) °	158.79(9)
Os – O(2) – Ni	175.4(12) °	161.3(4) °	161.0(4)
Os – O(3) – Ni	147.1(4) °	160.5(4) °	160.0(4)
$BVS_{(Ni)}$	+2.08	+1.98	+2.03
$BVS_{(Os)}$	+5.98	+5.91	+5.82

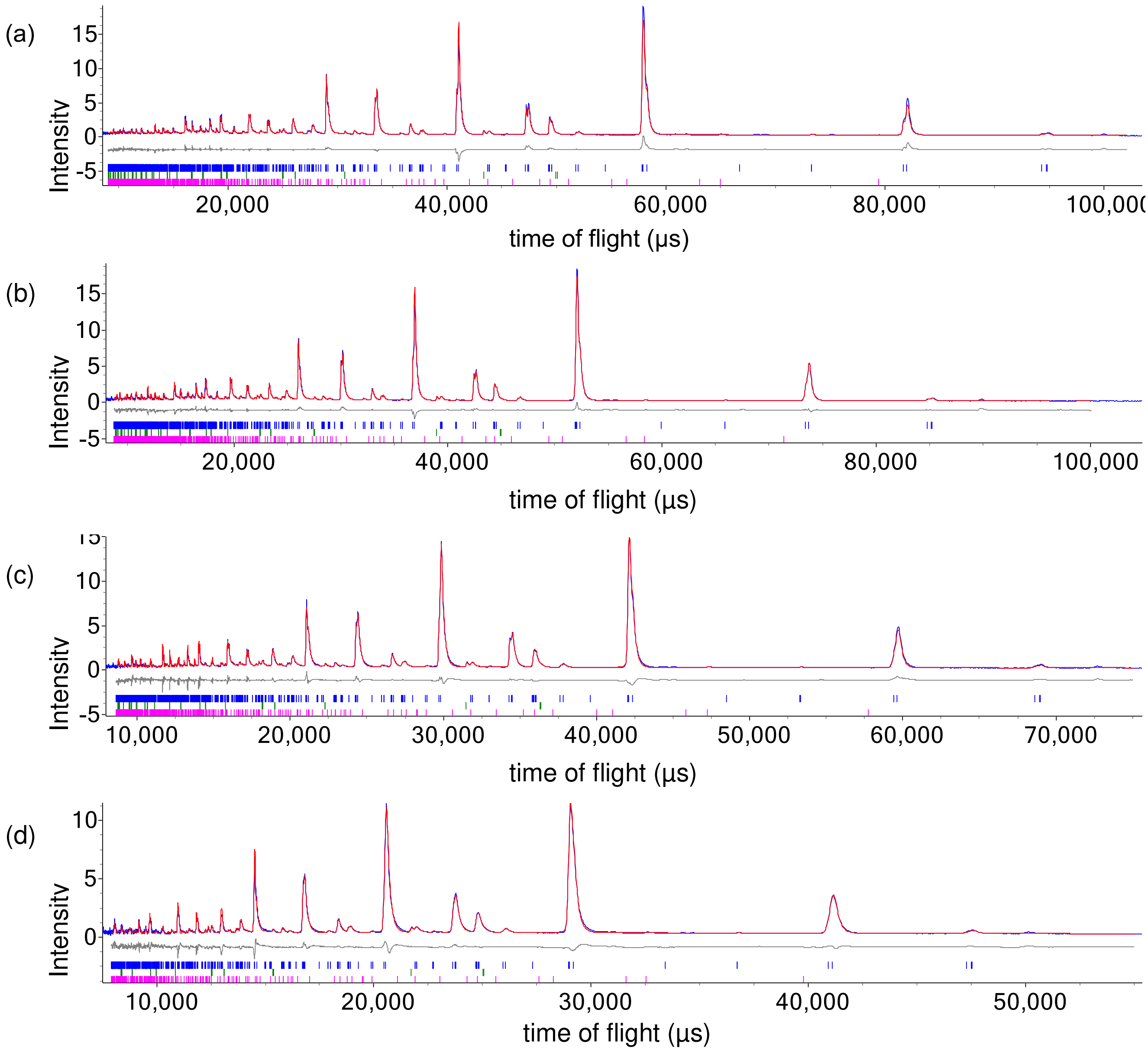

Figure S2a Refinement profiles (time of flight) for Pb_2NiOsO_6 using 98 K NPD data in space group $P2_1/n$ showing (a) higher resolution (153° bank) data, (b) 122° bank data, (c) 90° bank data and (d) 58° bank data. Observed, calculated and difference profiles are shown in blue, red and grey, respectively; upper (blue), middle (green) and lower (pink) ticks show reflection positions for the main phase Pb_2NiOsO_6 (98.86(4)% by weight) and impurity phases NiO (0.61(2)% by weight) and PbO_2 (0.53(3)% by weight), respectively.

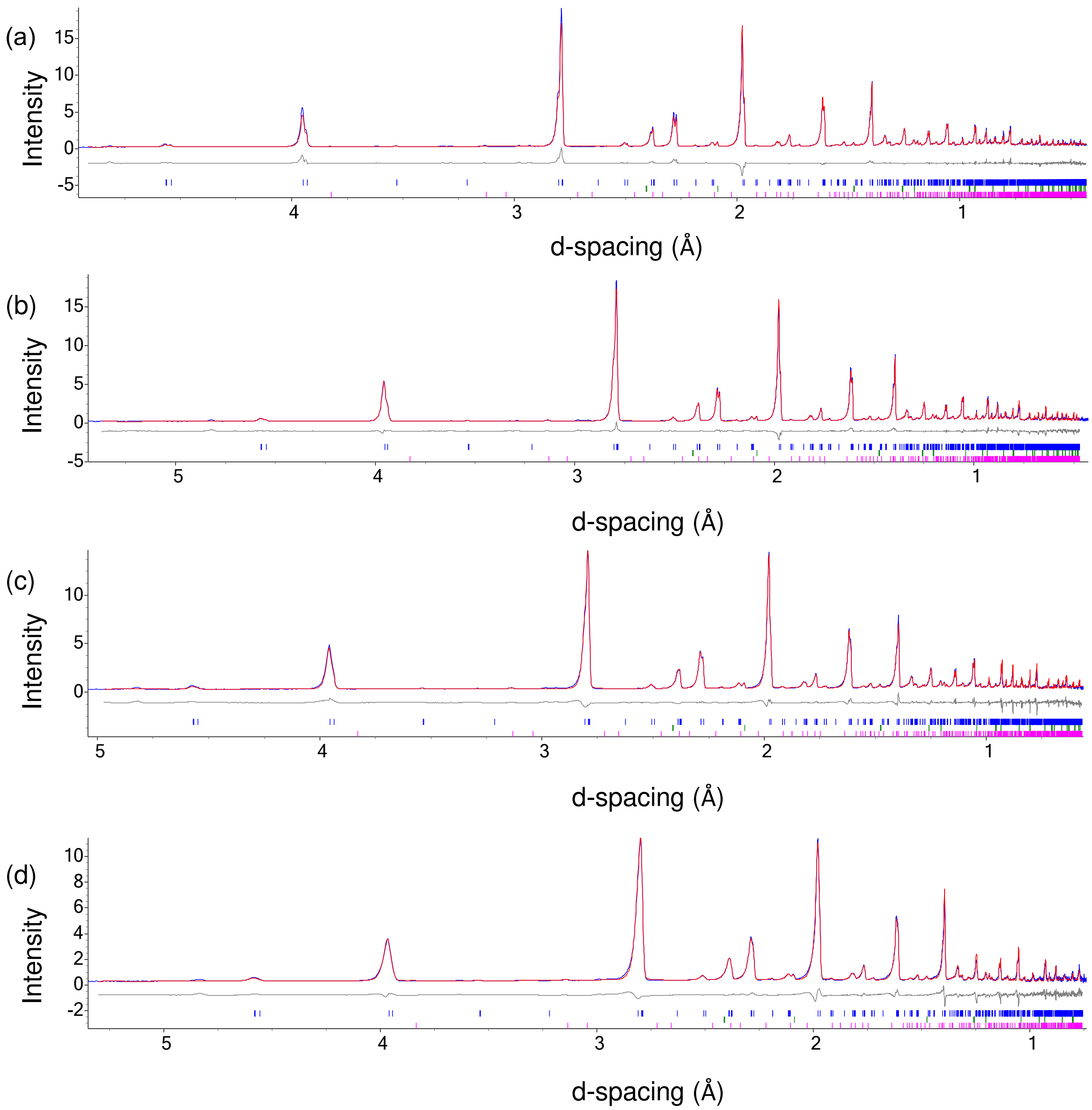

Figure S2b Refinement profiles (d-spacing) for Pb_2NiOsO_6 using 98 K NPD data in space group $P2_1/n$ showing (a) higher resolution (153° bank) data, (b) 122° bank data, (c) 90° bank data and (d) 58° bank data. Observed, calculated and difference profiles are shown in blue, red and grey, respectively; upper (blue), middle (green) and lower (pink) ticks show reflection positions for the main phase Pb_2NiOsO_6 (98.86(4)% by weight) and impurity phases NiO (0.61(2)% by weight) and PbO_2 (0.53(3)% by weight), respectively.

Table S3 Nuclear refinement details from Rietveld refinement of Pb_2NiOsO_6 using 98 K (upper values) and 1.5 K (lower values) NPD data in space group $P2_1/n$. At 98 K, cell parameters are a = 5.6134(1) Å, b = 5.5717(1) Å, c = 7.8757(2) Å, β = 89.956(4)°; R_{wp} = 6.07%, R_p = 6.70%. At 1.5 K, cell parameters are a = 5.60954(5) Å, b = 5.57031(4) Å, c = 7.87140(5) Å, β = 89.958(3)°; R_{wp} = 5.90%, R_p = 6.34%. The values obtained from 1.5 K NPD data are given on the second row for each atom.

Atom	site	*x*	*y*	*z*	Factional occupancy	U_{iso} × 100 (Å^2)	Magnetic moment (μ_B)
Pb	4*e*	0.0027(2) 0.0030(2)	0.5142(2) 0.5161(2)	0.2495(7) 0.2483(8)	0.970(1)† 0.970(1)†	0.90(2) 0.50(1)	- -
Ni	2*a*	0 0	0 0	0 0	1.00(6)† 1.00(6)†	1.07(2)* 0.74(1)*	- 1.90(1)
Os	2*b*	0 0	0 0	0.5 0.5	1.00(6)† 1.00(6)†	1.07(2)* 0.74(1)*	- 0.378(2)
O(1)	4*e*	-0.0635(2) -0.0647(2)	-0.0100(4) -0.0104(3)	0.2615(7) 0.2614(7)	0.988(3)† 0.988(3)†	0.91(7) 0.55(6)	- -
O(2)	4*e*	0.2342(7) 0.2315(8)	0.2854(8) 0.2850(8)	0.0323(9) 0.0328(9)	0.948(7)† 0.948(7)†	0.8(1) 0.5(1)	- -
O(3)	4*e*	0.2874(6) 0.2863(7)	0.7680(8) 0.7694(8)	0.0330(8) 0.0338(9)	1.013(7)† 1.013(7)†	1.5(1) 1.1(1)	- -

† occupancies fixed at values from refinement with a single global U_{iso} (see text)

* constrained to be identical

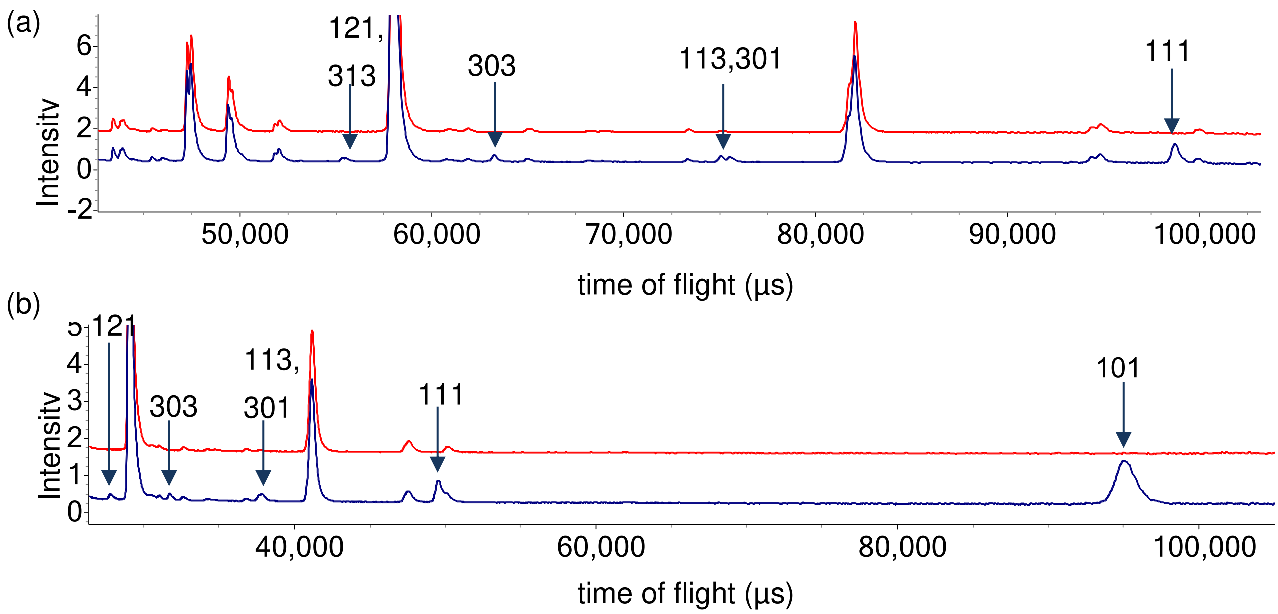

Figure S3 Raw NPD data for Pb_2NiOsO_6 collected at 98 K (red) and 2 K (blue) with additional magnetic reflections indexed by a magnetic unit cell with dimensions $2a_n \times b_n \times 2c_n$ (subscript n refers to the nuclear unit cell) showing (a) higher resolution (153° bank) data and (b) 58° bank data.

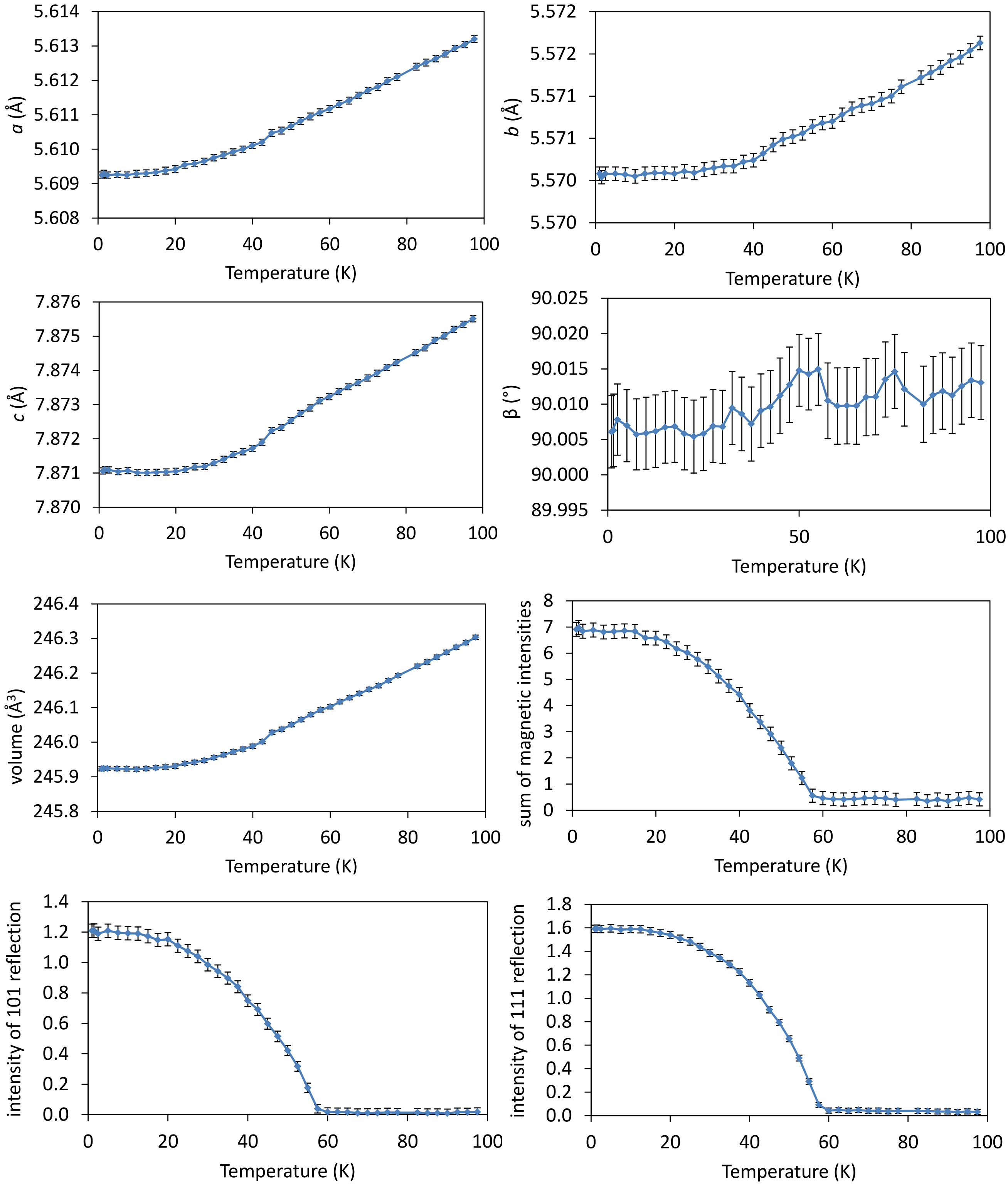

a (Å)
5.614
5.613
5.612
5.611
5.610
5.609
5.608
Temperature (K)
b (Å)
5.572
5.572
5.571
5.571
5.570
5.570
Temperature (K)
c (Å)
7.876
7.875
7.874
7.873
7.872
7.871
7.870
Temperature (K)
β (°)
90.025
90.020
90.015
90.010
90.005
90.000
89.995
Temperature (K)
volume (Å³)
246.4
246.3
246.2
246.1
246.0
245.9
245.8
Temperature (K)
sum of magnetic intensities
Temperature (K)
intensity of 101 reflection
Temperature (K)
intensity of 111 reflection
Temperature (K)

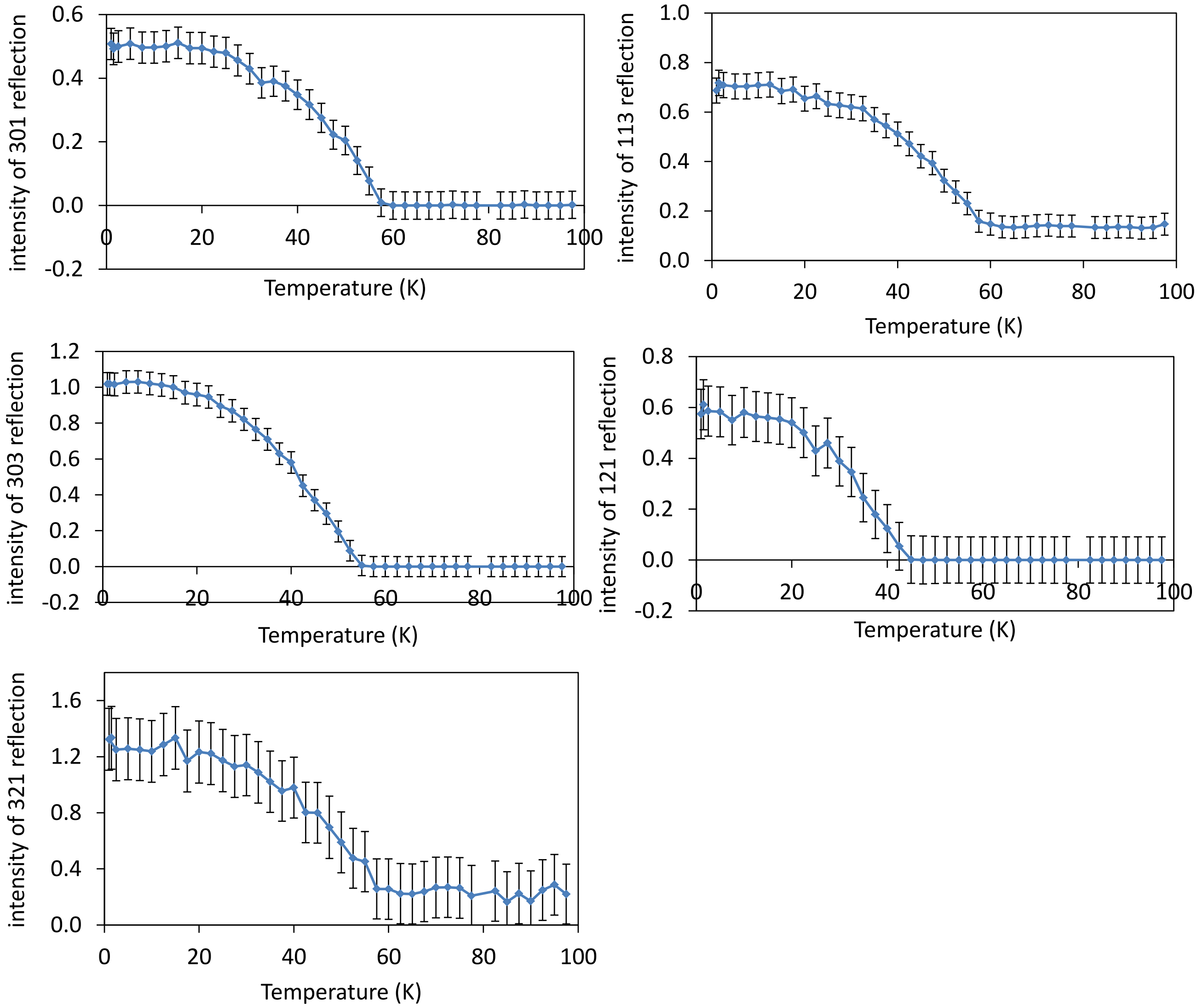

Figure S4 Evolution of magnetic peak intensity with temperature for Pb_2NiOsO_6 from sequential refinements using 58° bank NPD data: the nuclear phase was fitted with a Rietveld phase with unit cell parameters determined from refinement using high resolution (153° bank) data and the magnetic reflections were fitted with a Pawley phase with unit cell dimensions dimensions $2a_n \times b_n \times 2c_n$ (subscript *n* refers to the nuclear unit cell) and intensities of key reflections output.

Comparison of possible magnetic models and magnetic refinement details:

In addition to the Os mY_2^- magnetic order, allowing mY_1^+ moments on Ni sites and Γ_2^- displacements lowers R_{wp} from 6.42% to 5.99%, while allowing mY_2^+ moments on Ni sites and Γ_1^- displacements lowers R_{wp} to 5.97%. Attempts were made to follow the magnitude of the Γ_1^- and Γ_2^- displacements in sequential refinements to study their temperature dependence but any such displacements must be subtle and neither varied continuously with temperature.

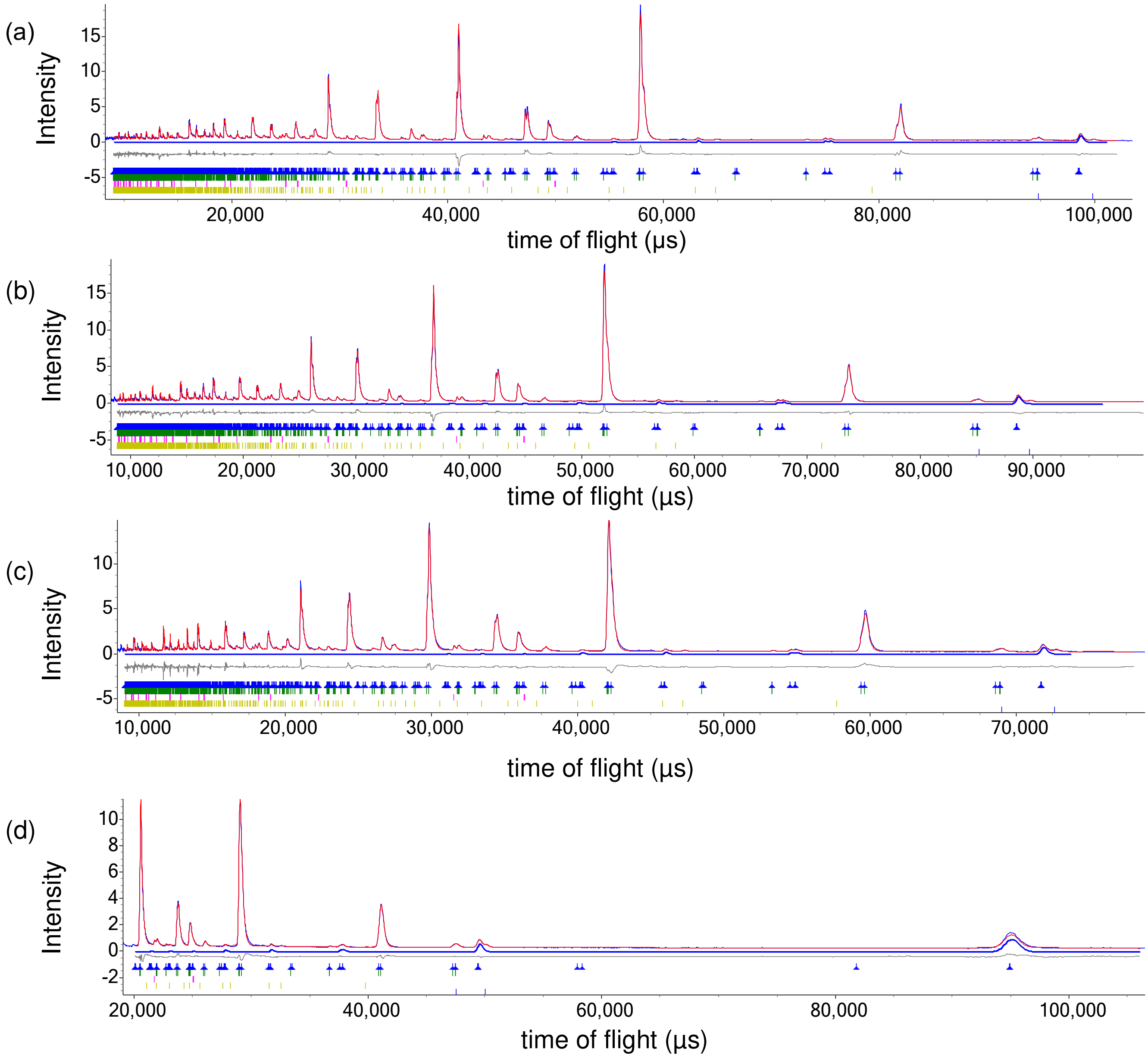

Figure S5a Refinement profiles (in time of flight) for Pb_2NiOsO_6 using 1.5 K NPD data in space group $P2_1/n$ showing (a) higher resolution (153° bank) data, (b) 122° bank data, (c) 90° bank data and (d) 58° bank data. Observed, calculated and difference profiles are shown in blue, red and grey, respectively and magnetic scattering is highlighted in blue. Top (blue), upper-middle (green), middle (pink), lower (yellow) and bottom (blue) ticks show reflection positions for the magnetic phase, the main phase Pb_2NiOsO_6 (~99% by weight), impurity phases NiO (~0.6% by weight), and PbO_2 (~0.5% by weight) and a Pawley phase to fit the two magnetic peaks of antiferromagnetic NiO, respectively.

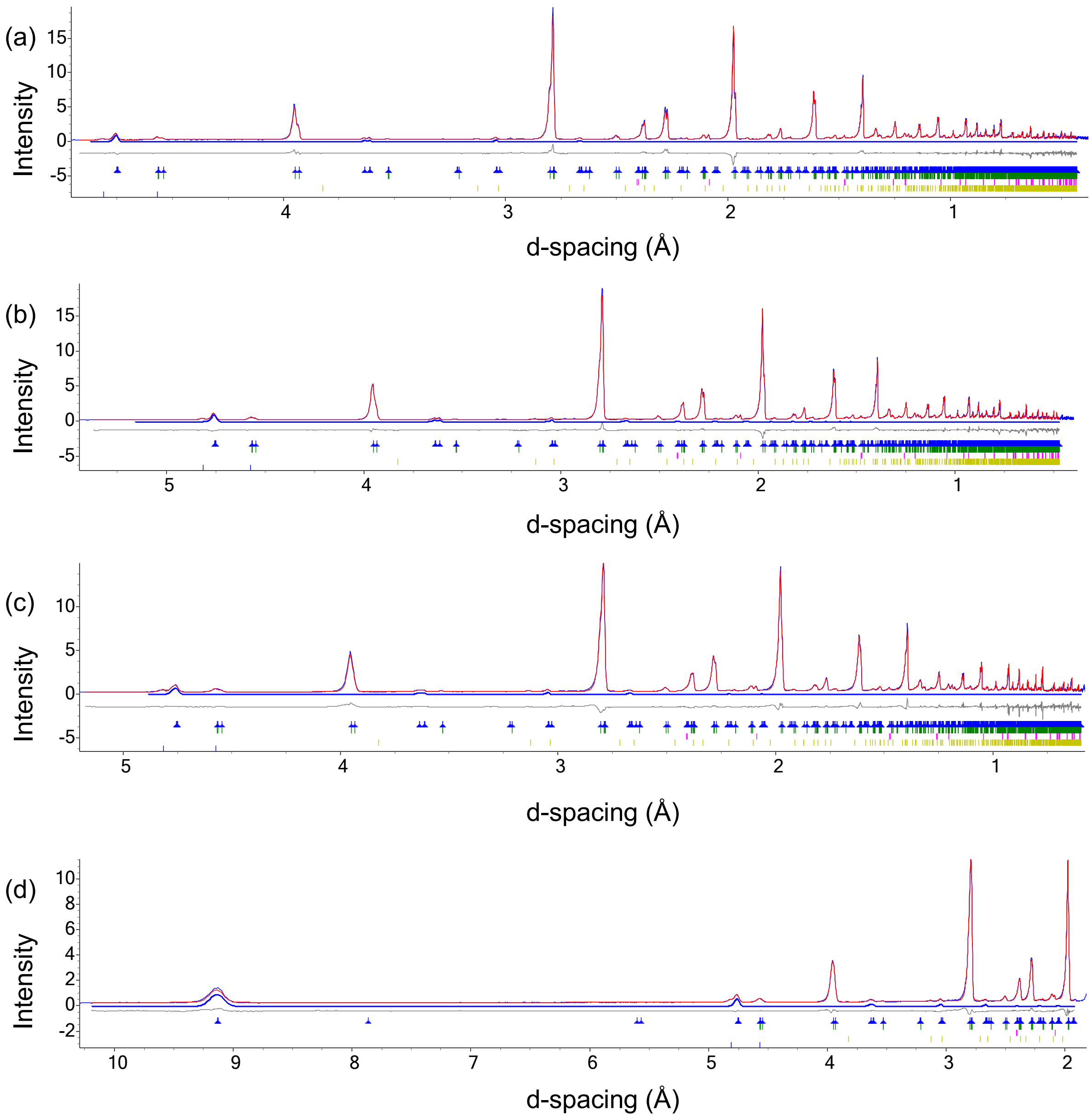

Figure S5b Refinement profiles (in d-spacing) for Pb_2NiOsO_6 using 1.5 K NPD data in space group $P2_1/n$ showing (a) higher resolution (153° bank) data, (b) 122° bank data, (c) 90° bank data and (d) 58° bank data. Observed, calculated and difference profiles are shown in blue, red and grey, respectively and magnetic scattering is highlighted in blue. Top (blue), upper-middle (green), middle (pink), lower (yellow) and bottom (blue) ticks show reflection positions for the magnetic phase, the main phase Pb_2NiOsO_6 (~99% by weight), impurity phases NiO (~0.6% by weight), and PbO_2 (~0.5% by weight) and a Pawley phase to fit the two magnetic peaks of antiferromagnetic NiO, respectively.

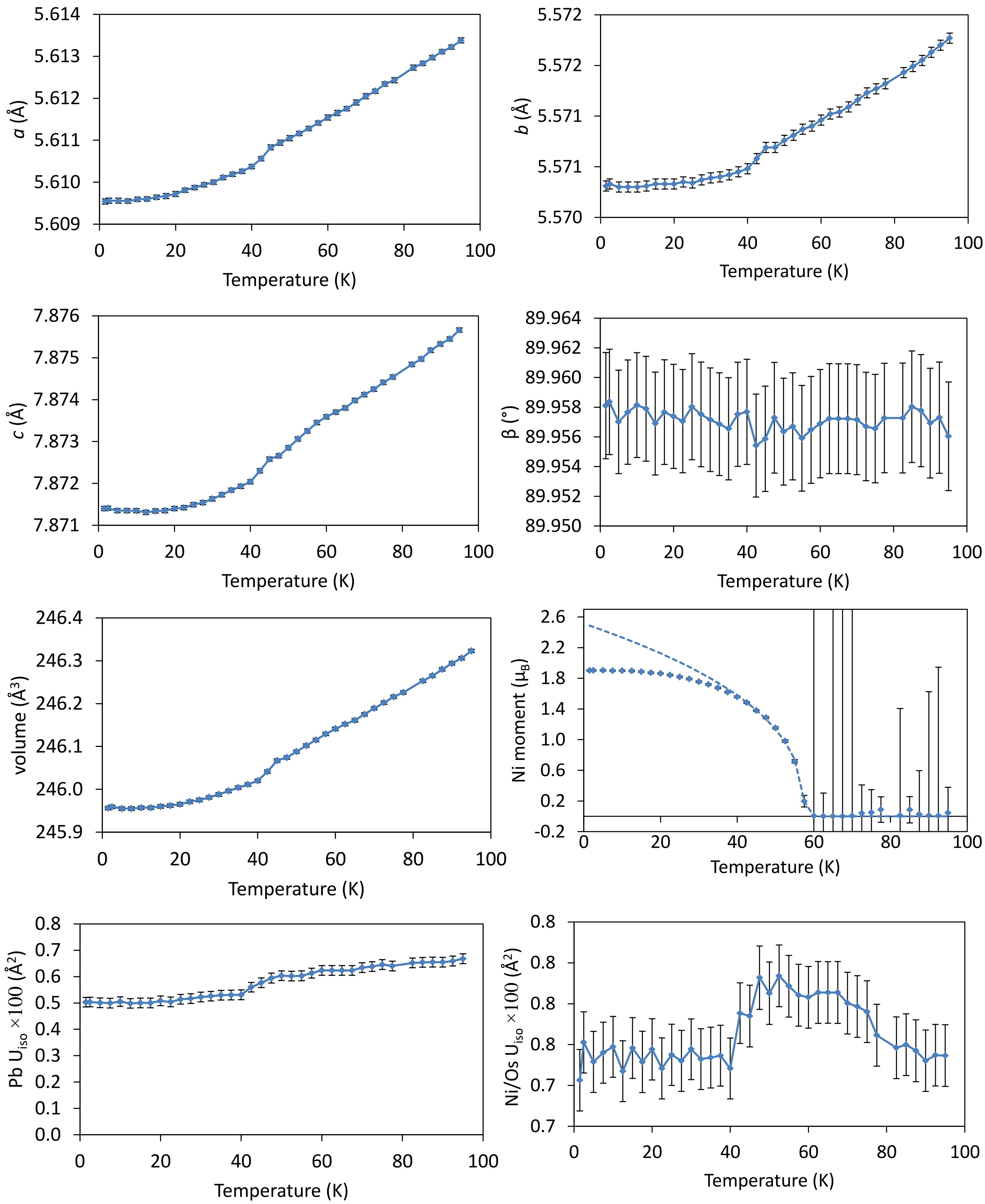

a (Å)
b (Å)
c (Å)
β (°)
volume (Å³)
Ni moment (μB)
Pb Uiso ×100 (Å²)
Ni/Os Uiso ×100 (Å²)
Temperature (K)

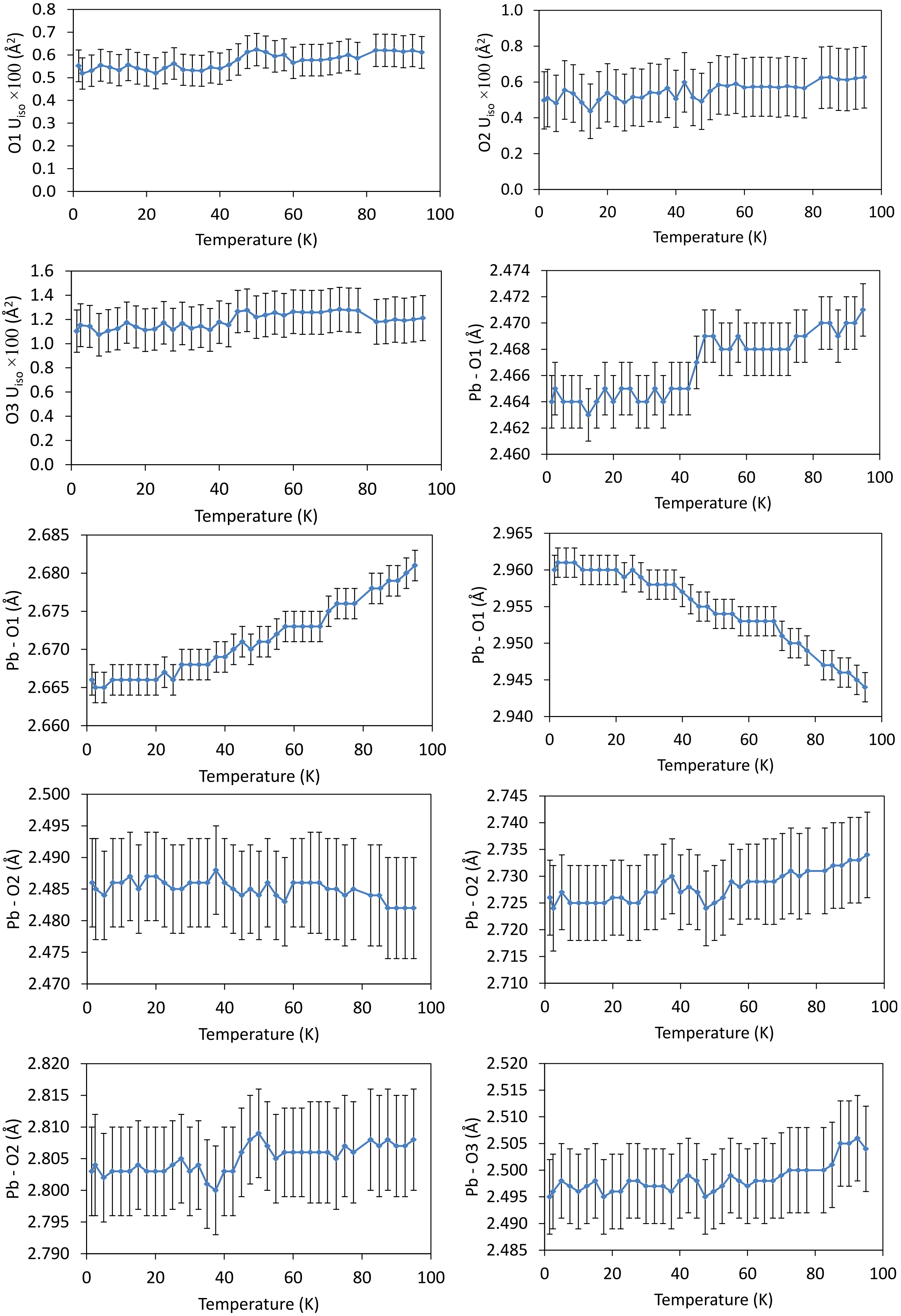

O1 U_{iso} ×100 (Å²)
O2 U_{iso} ×100 (Å²)
O3 U_{iso} ×100 (Å²)
Pb - O1 (Å)
Pb - O1 (Å)
Pb - O1 (Å)
Pb - O2 (Å)
Pb - O2 (Å)
Pb - O2 (Å)
Pb - O3 (Å)
Temperature (K)

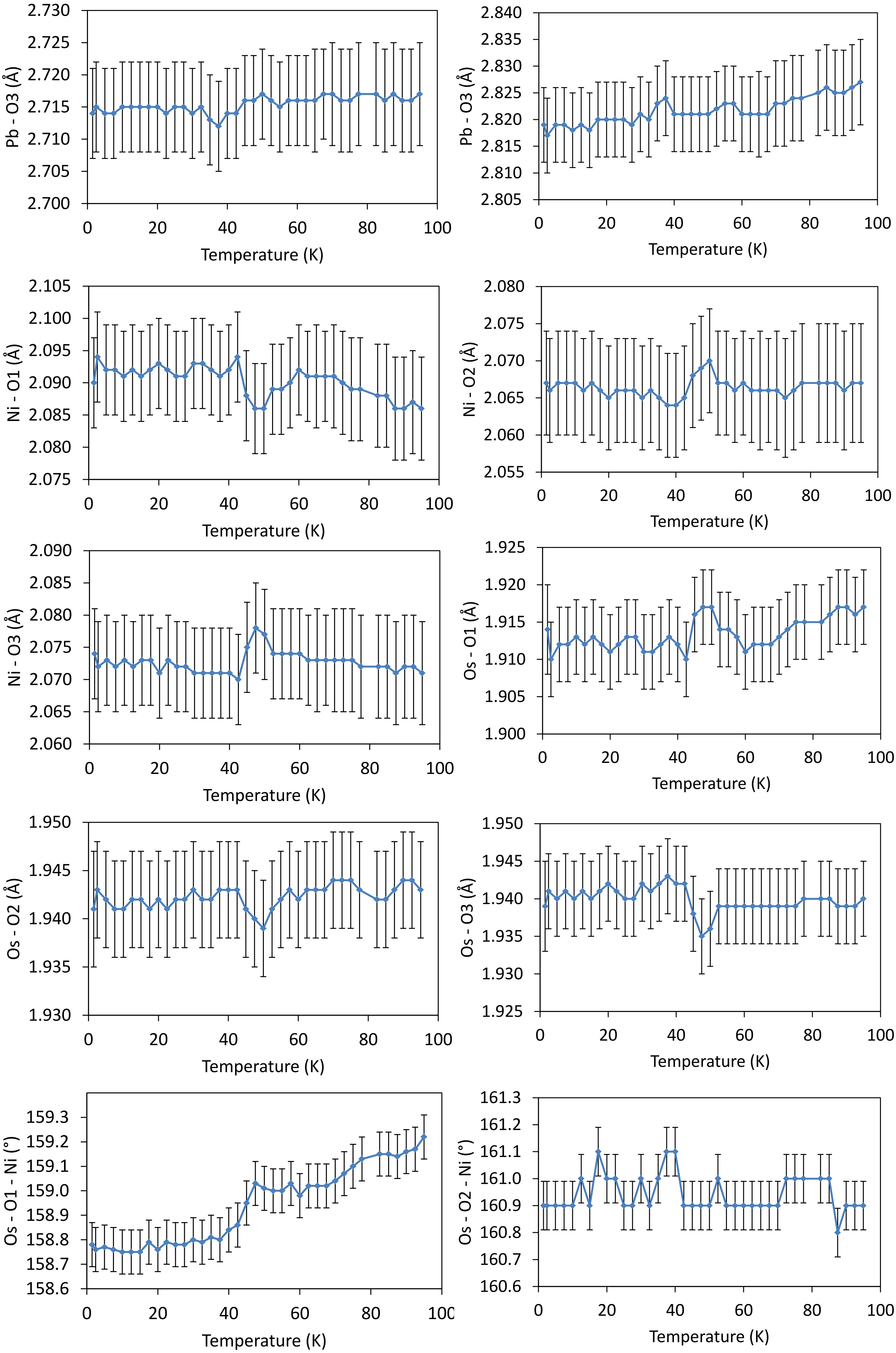

Pb - O3 (Å)
2.730
2.725
2.720
2.715
2.710
2.705
2.700
0 20 40 60 80 100
Temperature (K)
Pb - O3 (Å)
2.840
2.835
2.830
2.825
2.820
2.815
2.810
2.805
0 20 40 60 80 100
Temperature (K)
Ni - O1 (Å)
2.105
2.100
2.095
2.090
2.085
2.080
2.075
0 20 40 60 80 100
Temperature (K)
Ni - O2 (Å)
2.080
2.075
2.070
2.065
2.060
2.055
0 20 40 60 80 100
Temperature (K)
Ni - O3 (Å)
2.090
2.085
2.080
2.075
2.070
2.065
2.060
0 20 40 60 80 100
Temperature (K)
Os - O1 (Å)
1.925
1.920
1.915
1.910
1.905
1.900
0 20 40 60 80 100
Temperature (K)
Os - O2 (Å)
1.950
1.945
1.940
1.935
1.930
0 20 40 60 80 100
Temperature (K)
Os - O3 (Å)
1.950
1.945
1.940
1.935
1.930
1.925
0 20 40 60 80 100
Temperature (K)
Os - O1 - Ni (°)
159.3
159.2
159.1
159.0
158.9
158.8
158.7
158.6
0 20 40 60 80 100
Temperature (K)
Os - O2 - Ni (°)
161.3
161.2
161.1
161.0
160.9
160.8
160.7
160.6
0 20 40 60 80 100
Temperature (K)

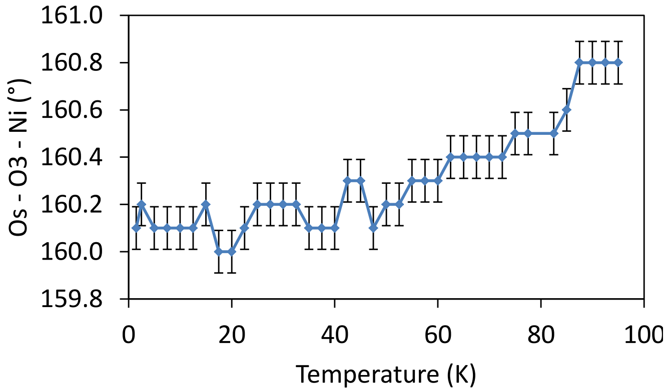

Figure S6 Evolution of nuclear and magnetic structures with temperature for Pb_2NiOsO_6 from sequential refinements using NPD data from higher resolution (153°) bank, 122° bank, 90° bank data and 58° bank data. The nuclear phase was fitted with a Rietveld phase, as was the magnetic-only phase with unit cell parameters constrained to be related to the nuclear unit cell.

The unit cell volume contracts a little more rapidly on cooling below ~40 K and this coincides with a change in the slope of some bond lengths and angles (a Pb – O1 and the Os – O1 – Ni bond angle) as the O(1) site moves in the negative *x* direction. We note that the weakest magnetic reflection, 121, appears to increase in intensity only below ~40 K and there may be a slight change in magnetic structure (and a concomitant change in the crystal structure) at this temperature. Possible changes in the magnetic structure include ordering of a second magnetic sublattice e.g. if Ni^{2+} moments ordered at T_N and Os^{6+} moments ordered below ~40 K, or if some reorientation of moments occurred below ~40 K. Mode inclusion analysis[1, 2] using 47.5 K data gave qualitatively similar results to that carried out at low temperature (indicating the same magnetic structure). Likewise, refinements using 47.5 K data allowing the magnetic moment direction to refine freely, and constraining the moments to lie along the $P2_1/n$ [001] direction gave very similar fits (R_{wp}s of 5.938% and 5.936% for the constrained and free models, respectively) and the unconstrained model resulted in moments lying very close to the $P2_1/n$ [001]. Due to the low intensity of the 121 reflection, it's hard to determine whether it is present for 40K ≤ T ≤ T_N. Given the high correlation in the refinement between moments on the two cation sites, it may not be possible to resolve this question from powder diffraction data, and given the magnetic susceptibility and heat capacity data, we must assume a single magnetic ordering transition at T_N.

Further details regarding DFT calculations:

The magnetic ground state of Pb_2NiOsO_6 was studied by calculating the total energy for each of the different magnetic states, namely FM, AFM-1, and AFM-2 (see Figure S7). Both Ni and Os moments order in AFM-1, which leads to inversion symmetry break. On the other hand, only Ni moments order in AFM-2 and inversion symmetry is preserved. From the total energy calculations (see Table 2), AFM-1 is found to have the lowest energy, with an energy difference of 0.102 eV/formula unit from that of AFM-2, thereby suggesting that DFT calculations favor the noncentrosymmetric AFM model with AFM order on both Ni and Os sublattices.

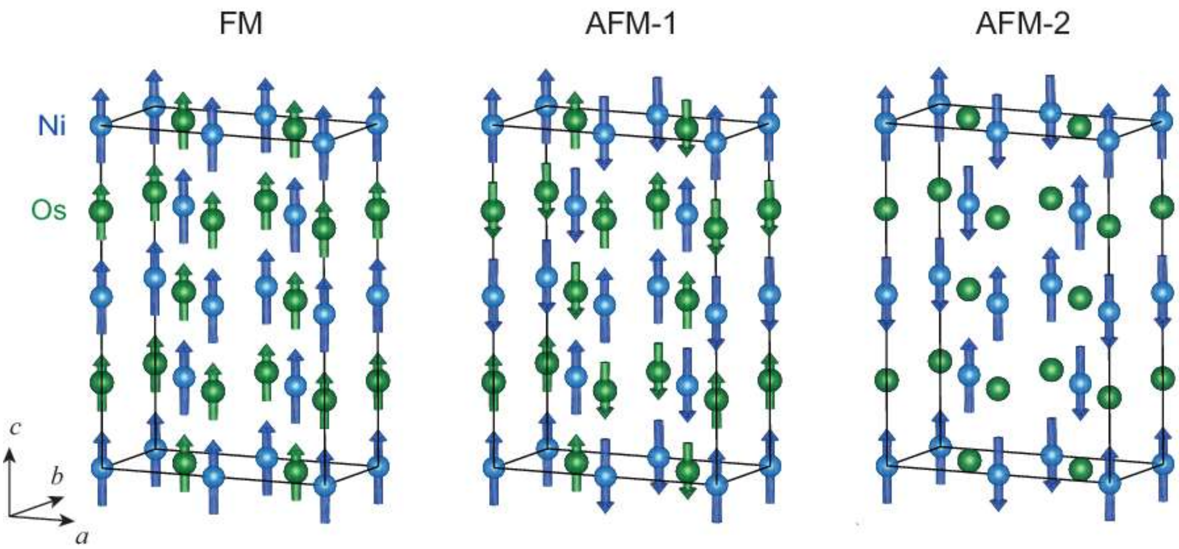

Figure S7 Possible spin arrangement considered in the theoretical calculation for Pb_2NiOsO_6; ferromagnetic (FM), antiferromagnetic AFM-1 and AFM-2 configurations. Ni and Os atoms are only shown for clarity.

Table S4 The total energy calculated for Pb_2NiOsO_6 with different magnetic states

Magnetic phase	Total energy (eV/formula unit)
AFM-1	0
AFM-2	+0.102
FM	+1.880

DFT calculations were carried out on the four magnetic models (models 1 – 4, see main text) to investigate their relative energies. Details of these models including basis vectors and origin shifts relative to the nuclear $P2_1/n$ structure are given below.[3]

Model 1:
Ni: mY_2^+
Os: mY_2^-
Polar distortion: Γ_1^-
Magnetic symmetry: P_a2_1
Basis vectors: (200) (010) (-101)
Origin shift: (-¼ 0 ¼)

Model 2:
Ni: mY_1^+
Os: mY_2^-
Polar distortion: Γ_2^-
Magnetic symmetry: P_ac
Basis vectors: (-200) (0-10) (101)
Origin shift: (0 ¼ 0)

Model 3:
Ni: mY_1^+
Os: mY_1^-
Polar distortion: Γ_1^-
Magnetic symmetry: P_a2_1
Basis vectors: (200) (010) (-101)
Origin shift: (-¼ 0 -¼)

Model 4:
Ni: mY_2^+
Os: mY_1^-
Polar distortion: Γ_2^-
Magnetic symmetry: P_ac
Basis vectors: (200) (010) (-101)
Origin shift: (0 ¼ 0)

References

1. McCabe, E. E.; Stock, C.; Rodrigues, E. E.; Wills, A. S.; Taylor, J. W.; Evans, J. S. O., Weak spin interactions in Mott insulating $La_2O_2Fe_2OSe_2$. *Phys. Rev. B* **2014,** *89*, 100402(R).
2. Tuxworth, A. J.; McCabe, E. E.; Free, D. G.; Clark, S. J.; Evans, J. S. O., Structural Characterization and Physical Properties of the New Transition Metal Oxyselenide $La_2O_2ZnSe_2$. *Inorg. Chem.* **2013,** *52*, 2078-2085.
3. Campbell, B. J.; Stokes, H. T.; Tanner, D. E.; Hatch, D. M., ISODISTORT. *J. Appl. Cryst.* **2006,** *39*, 607-614.